A THESIS

On

EFFECT OF La^{3+} AND Gd^{3+} FOR Bi^{3+} IN BISMUTH VANADATE ELECTROLYTE

Submitted in the partial fulfillment of requirement for the award of the degree of

Master of Technology (M. Tech)

IN

MATERIALS SCIENCE AND ENGINEERING

Submitted by

DEEPTI
Roll No. : 6040502

Under the guidance of

Dr. KULVIR SINGH
Assistant Professor

School of Physics and Materials Science

THAPAR INSTITUTE OF ENGINEERING AND TECHNOLOGY

(DEEMED UNIVERSITY)

PATIALA (PUNJAB)-147004

JUNE 2006

CERTIFICATE

This is to certify that the thesis entitled **EFFECT OF LA^{3+} AND GD^{3+} FOR Bi^{3+} IN BISMUTH VANADATE ELECTROLYTE** submitted by **Miss Deepti** in the partial fulfillment of the requirement for the award of the degree of **M. Tech** in **Materials Science and Engineering** from the **School of Physics and Materials Science, Thapar Institute of Engineering and Technology (Deemed University), Patiala,** is a record of candidate's own work carried out by her under my supervision and guidance. The matter embodied in this report has not been submitted in part or full to any other university or institute for the award of any degree.

(Dr.Kulvir Singh)

Assistant Professor, SPMS

Thapar Institute of Engg. &Technology, Patiala, Punjab (147004)

Countersigned by:

(Dr. O.P. Pandey)
Professor and Head, SPMS
Thapar Institute of Engg. & Technology,
Patiala, Punjab (147004)

(Dr. T.P. Singh)
Dean, Academic Affairs
Thapar Institute of Engg. & Technology,
Patiala, Punjab (147004)

Dated:

ACKNOWLEDGEMENTS

I express my deep gratitude and respects to my guide **Dr. Kulvir Singh**, **Assistant Professor** for his keen interest and valuable guidance, strong motivation and constant encouragement during the course of the work. I thank him from the bottom of my heart for introducing me to the science of fuel cells. I thank him for his great patience, constructive criticism and myriad useful suggestions apart from invaluable guidance to me.

I am grateful to **Dr. O.P. Pandey, Professor and Head, School of Physics and Materials Science** for his encouragement and execution of thesis work.

I would also like to thank **Dr. K. K. Raina, Professor and Dean Resource Planning and Generation,** for his constant guidance and encouragement.

It gives me immense pleasure to express my special thanks to **Mr Ravi Kant** who always took keen interest in guiding me during my work. I wish my sincere thanks to **Ms Anu Arora** for their cooperation.

I owe my sincere thanks to all the staff members of **School of Physics and Materials Science** for their support and encouragement.

I would also like to thank my marvelous friends **Ms Himani, Ms Komal, Ms Shallu Thakur, Ms Gurpreet, Mr. Inderpreet, Mr. Mohit, Mr. Vishal,** and **Mr. Sameer** for extending their whole hearted support.

Last but not the least; I would like to thank my parents, my sister and brother for their moral support that kept my spirit up during the endeavor.

Deepti

Roll No. 6040502

Dedicated To My Parents

CONTENTS PAGENUMBER

LIST OF ACRONYMS

SOFC	Solid Oxide Fuel Cell
PAFC	Phosphoric Acid Fuel Cell
AFC	Alkaline Fuel Cell
PEM	Proton Exchange Membrane
DMFC	Direct Methanol Fuel Cell
MCFC	Molten Carbonate Fuel cell
HUMO	highest unoccupied molecular orbital
LUMO	lowest unoccupied molecular orbital
YSZ	yttria-stabilized zirconia
GDC	gadolinia-doped ceria
BIMEVOX	metal cation substituted bismuth vanadate
IT	intermediate temperature
XRD	x-ray diffraction
D	differential thermal analysis
DSC	differential scanning calorimetry
ac	alternate current

LIST OF SYMBOLS

d	interplanner distance
K	Kelvin
nm	nanometer
μ	mobility
Ω	ohm
R	resistance
ρ	resistivity
σ	conductivity
t	transport number
^{o}C	temperature
^{o}A	Angstrom
S	Siemen
a, b, c	lattice parameter
C	capacitance
ε	permitivity

ABSTRACT

The modern scientific and technological approach, in the area of energy production is to develop inexpensive devices, which could satisfy the current drive for cleaner and more efficiently distributed power, particularly in combination of heat and power systems. In this context, fuel cells represent a promising and viable alternative for large scale generation of electricity, with minimal undesirable chemical, thermal and acoustic emissions. A fuel cell is a device that directly converts the chemical energy of reactants (a fuel such as hydrogen, natural gas, methane or methanol and an oxidant air or oxygen), into electricity. Solid Oxide Fuel Cell (SOFC) is the most advancing field in the science of fuel cell due to higher efficiency than other fuel cells. The obstacle in the commercialization of SOFCs is their high operating temperature. Solid electrolyte is the most important part of SOFCs. Its performance is critical to the development and commercialization of SOFC. Therefore several efforts have been made to develop a suitable solid electrolyte which has higher ionic conductivity in intermediate temperature range (800- 600^{o}C).

Several electrolyte materials have been studied and it is found that bismuth oxide based electrolytes shows higher conductivity at lower temperatures when doped with various aliovalent cations. Basically, bismuth vanadate exhibits three phase transition i.e. $\alpha \rightarrow \beta$ and $\beta \rightarrow \gamma$ in room temperature to 700^{o}C temperature range. In these phases disordered γ-phase shows higher conductivity than α and β phases. γ-phase could be stabilized at room temperature after doping of various cations. In present study, a series of $Bi_{4-x}M_xV_2O_{11}$ ($0 \leq x \geq 0.4$; M= Gd, La) have been synthesized and characterized by using various techniques such as X-ray diffraction, Differential scanning calorimetry (DSC), Thermogravimetric analysis (TGA) and ac conductivity measurement. All the samples exhibit either α-$Bi_4V_2O_{11}$ or β-$Bi_4V_2O_{11}$ phase. These phase formations is further confirmed by DSC and ac conductivity measurement. The conductivity variation has been discussed on the base of defect mechanism.

CHAPTER 1

INTRODUCTION

1.1 Solid electrolytes

An electrolyte is a substance which dissociates free ions when dissolved. Because they generally consist of ions in solution, electrolytes are known as ionic solutes. Electrolytes find their primary application in electrochemical cells. Solid electrolytes are particularly useful where the reactants of the electrochemical cell are either gaseous or liquid.

In solid electrolytes, cation or anion is not confined to specific lattice sites but is essentially free to move throughout the structure. Solid electrolytes are therefore, intermediate in structure and property between, normal crystalline solids and liquids. Often solid electrolytes are stable only at high temperatures. At lower temperatures they may undergo a phase transition to give a polymorph with a low ionic conductivity and a more usual type of crystal structure. For example, Li_2SO_4 and AgI are both poor conductors at 25^oC but at temperatures of 572 and 146^oC, respectively, their crystal structures changes to give a polymorphs, α- Li_2SO_4 and α- AgI, that have mobile Li^+ and Ag^+ ions ($\sigma \sim 1 Scm^{-1}$). On heating, the conductivity therefore increases dramatically due to phase transition.

Secondly, solid electrolytes form as a consequence of a gradual increase in defect concentration with increasing temperature. For example, in ZrO_2, the concentration of anion vacancies above $\sim 600^oC$ is sufficiently large that zirconia becomes good ionic conductor.

1.2 Various Solid electrolytes

1.2.1 β- alumina

β-alumina is the name of a family of $M_2O.nX_2O_3$ where n can have various values in the range 5 to 11, M is a monovalent cation, such as alkali Li^+, Cu^+, Ag^+, Ga^+, In^+, Tl^+, NH_4^+ and X is a trivalent cation, Al^{3+}, Ga^{3+} or Fe^{3+}. The most important member of this family is sodium β-alumina ($M=Na^+$, $X=Al^{3+}$), which has been known for many years as a byproduct of the glass making industry. Interest in β-alumina as a solid electrolyte began with the pioneering work of the Ford Motor Co. in 1966[1], they reported that the Na^+ ions are very mobile at room temperature and above in β-alumina.

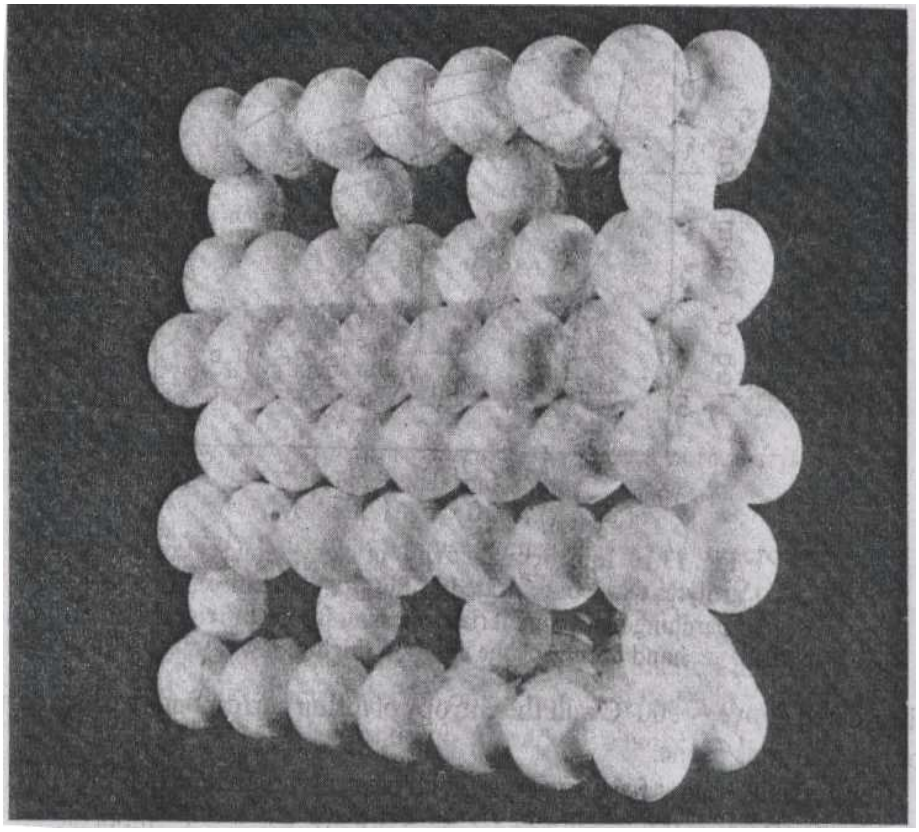

Figure 1.1: *Oxide layers in β-alumina*

The high conductivity of the monovalent ions in β-alumina is a consequence of its unusual crystal structure as shown in Fig.1.1. It exhibits closed packed layers of oxide ions, stacked in three dimensions, but every fifth layer has three quarters of oxygen deficiency. The sodium ions reside in the oxygen-deficient layers and are able to move very easily because (a) there are more sides available than there are Na^+ ions to occupy them and (b) the radius of Na^+ is less than that of O^{2-} ion. β-alumina exists in two structural modifications, named β and β″ which are differing in stacking sequence of layers. The β″ forms occur with more soda rich crystal, n ≈ 5-7, whereas β occurs for n ≈8-11. Both β and β″ structures are closely related to that of spinel, $MgAl_2O_4$; Al^{3+} ions occupy a selection of both tetrahedral and octahedral interstices between pairs of adjacent closed packed oxide layers. Both β- andβ″-alumina structures may be regarded as a built of 'spinel blocks' that are four oxide layer thick and in which the oxide layers are in cubic stacking sequence ABCA. Adjacent spinel blocks are separated by the oxygen-deficient layers or 'conduction planes' in which the Na^+ ion

reside. The unit cell is hexagonal with a=5.60A^{o} and c=22.5 (β), 33.8A^{o} (β″). In the c direction, perpendicular to the oxide layers, there are two spinel blocks in the unit cell of β and three blocks in the unit cell of β″. The structure of 'spinel block' must be considered as defective in comparison with the ideal spinel structure.

β-alumina is a two dimensional conductor. Alkali ions are able to move freely with in the conduction planes but cannot penetrate the dense, spinel blocks. The conductivity of different single crystal β-alumina in directions parallel to the conduction planes is shown in Fig.1.2. Much of the work has been reported [1] on β rather than β″ because good quality single crystals have been available only for the β crystal form; however the conductivity of β″ is greater than that of β by a factor of 2 to 3. With increasing cation size (K^+, Tl^+); conduction becomes more difficult since the larger cations cannot move as readily within the conduction planes Na^+ and Ag^+ appear to have the optimum size because Li^+ β-alumina also has a higher activation energy and lower conductivity than Na^+ or Ag^+ β-alumina. In this case, Li^+ ions appear to occupy sites in the walls of the conduction plane; Li^+ is a small, highly polarizing cation unlike Na^+.

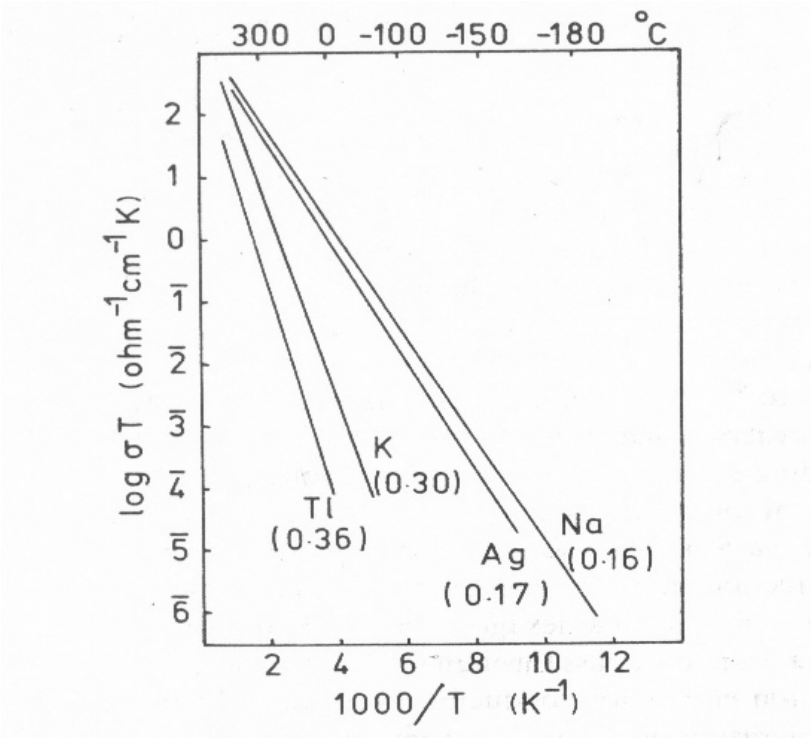

Figure 1.2: *Conduction of some single crystal β-alumina*

1.2.2 AgI and Ag^+ ion solid electrolytes

AgI undergoes a phase transition at 146^{o}C and having exceptionally high conductivity of the order (~1Scm^{-1}) which is about four orders of magnitude larger than the room temperature value. The activation energy for conduction in α-AgI is only 0.05eV.

β-AgI, is stable in the temperature range below 146^{o}C, has the wurtzite with hexagonal close packed I^- ions and Ag^+ in tetrahedral sites. Another low temperature polymorph is γ-AgI; its structure is that of sphalerite. The highly conducting, high temperature α polymorph is body centred cubic in which iodide ions lie at the corner and body centred positions whereas Ag^+ ions are distributed statistically over a total of thirty-six sites of tetrahedral and trigonal coordination. The tetrahedral sites are linked together by sharing faces and trigonal sites lie at the center of the faces of the AgI_4 tetrahedra. The iodide ions are essentially fixed and Ag^+ ions can readily move from one side to the next in a liquid-like manner. The disordered Ag^+ arrangements and the easy motion of Ag^+ between sites must be related to the nature of bonding between silver and iodine. Silver is a polarizing cation since its outer 4d electrons are relatively ineffective in shielding nuclear charge. Iodide is a large and polarizable anion and so covalent bonds readily form between Ag^+ and I^- that are characterized by structures with low coordination numbers. During conduction, silver can readily move from one tetrahedral site to next via an intermediate, three-coordination site. Covalent bonding at the intermediate site helps to stabilize it and reduce the activation energy for conduction. It has been reported [1] that AgCl and AgBr have reasonable conductivities at high temperatures-but lower than that of AgI because of less percent of covalent bonding as compared to AgI.

In an attempt to stabilize the highly conducting α-AgI phase at lower temperatures, various anionic and cationic substitutions have been reported [1]. The most successful so far has been the partial replacement of silver by rubidium in $RbAg_4I_5$. This material has the highest ionic conductivity at room temperature of any known crystalline substance (0.25 Scm^{-1}) as shown in Fig. 1.3. Its activation energy for conduction is 0.07eV. The amount of electronic conductivity in $RbAg_4I_5$ is negligibly small (~10^{-9} Scm^{-1}) at 25^{o}C. The phase diagram for the system RbI-AgI is shown in Fig 1.4.

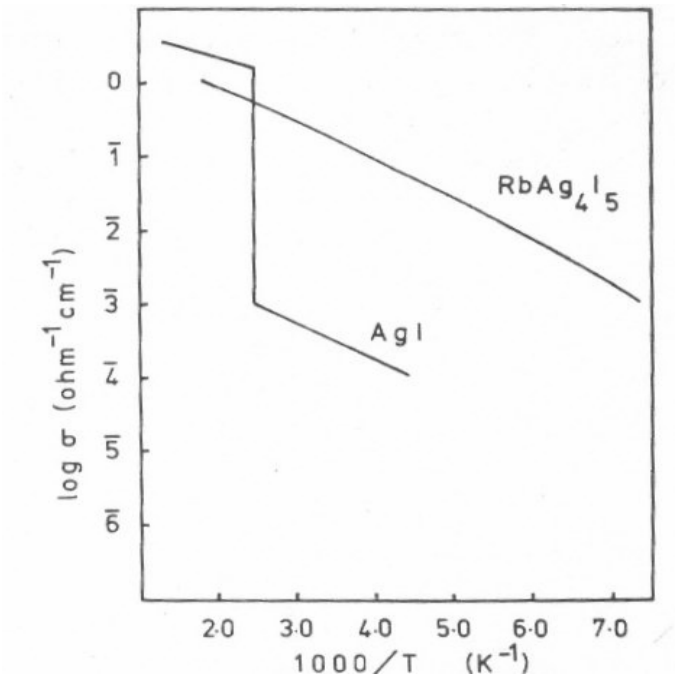

Figure 1.3: *Conductivity of Ag^+ in AgI and $RbAg_4I_3$*

The crystal structure of $RbAg_4I_3$ is rather different to that of α-AgI, but it also contains a random arrangement of silver atoms distributed over a network of face sharing tetrahedral sites. Again there are many more available sites then there are silver atoms to fill them. Rubidium atoms are immobilized in sites that have a distorted octahedral environment of I^- ions.

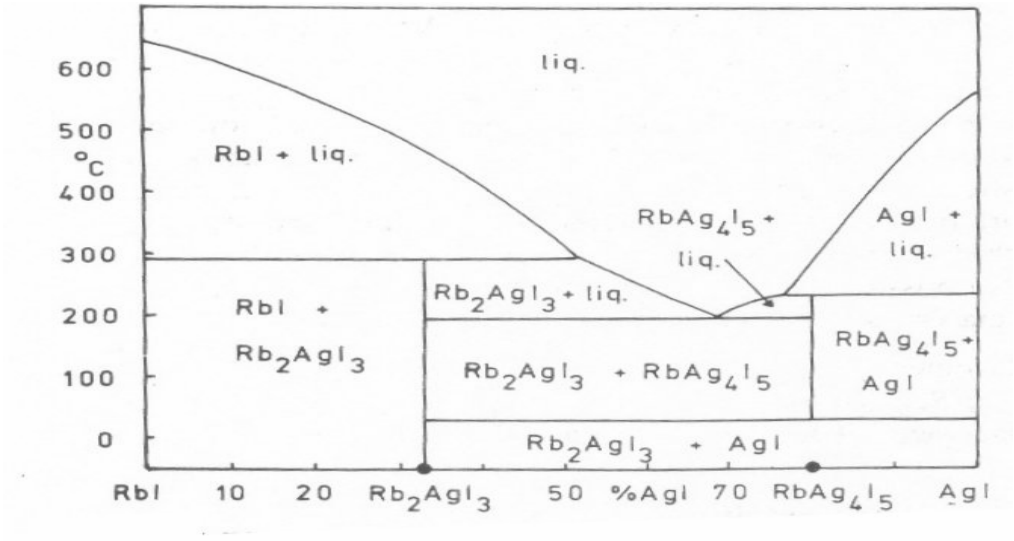

Figure 1.4: *Phase diagram for AgI-RbI*

1.2.3 Halide ion conductors

Several halides that have the fluorite (CaF_2) structure may be classified as solid electrolytes at high temperatures because they have high halide ion conductivity. One of the best examples is PbF_2 in which $\sigma \approx 5$ ohm^{-1}cm^{-1} above 500^{o}C [1]. At room temperature, PbF_2 has a very low ionic conductivity as seen from Fig.1.5. With increasing temperature its conductivity increases rapidly until at ~ 500^{o}C. Above this temperature σ increases only slowly and there is little change in σ upto its melting (822^{o}C) [1]. It is interesting that some ionic conductors such as PbF_2 arrive in the highly conduction condition gradually on increasing the temperature, whereas other materials such as AgI do so by undergoing an abrupt change in crystal structure.

The fluorite structure may be described in various ways; one of them is primitive cubes of F^- ions with Ca^{2+} ions at the body centers of alternate cubes. The sites available for interstitial F^- at the centers of the alternate cubes; these sites are normally coordinated by six calcium in an octahedral arrangement and eight fluorines at the cube corners. In creating an interstitial F^- ion, one of the corner F^- ions must move off its corner site and into the body of the cube.

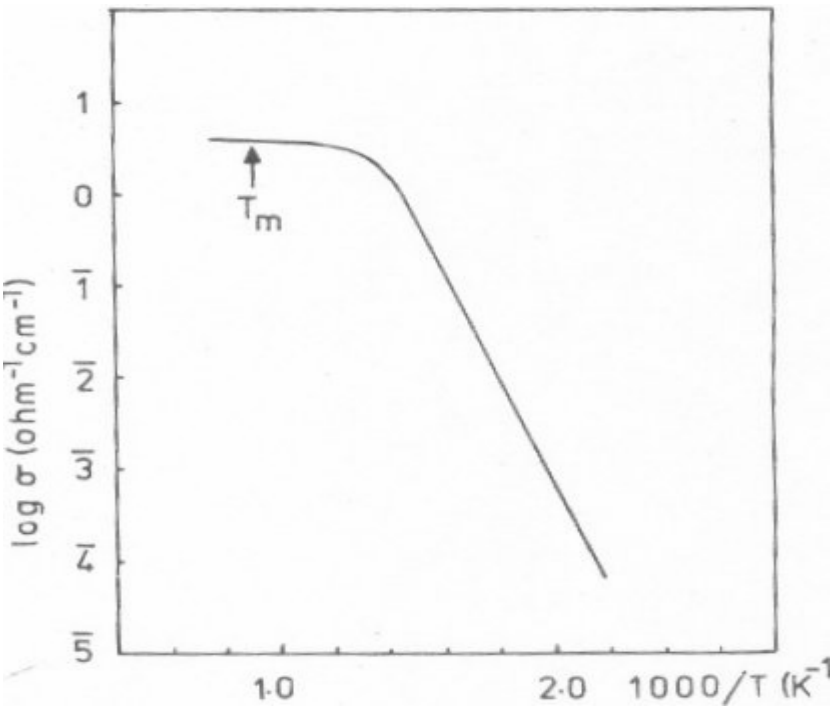

Figure 1.5: Conductivity of PbF_2

1.2.4 Oxide ion conductors

Ideally, an oxide – ion conductor conducts only O^{2-} ions and remains an electonic insulator under operating conditions. Oxide ion electrolytes are oxides, and the constraints on their ability to remain electronic insulators depend on the application in which they are used. For example at high temperature, cubic polymorph of zirconia has the fluorite crystal structure. This phase can be stabilized by formation of solid solutions with CaO, Y_2O_3 at room temperature. Stabilized zirconia is good O^{2-} ion conductors at high temperatures, mainly because the mechanism of solid solution formation involves the creation of vacant O^{2-} sites in order to achieve electroneutrality. The fluorite crystal structure appears to be

particularly suitable for high ionic conductivity. Typical conductivities in stabilized zirconias (e.g.85 mol% ZrO_2, 15% CaO) are $5x10^{-2}$ Scm^{-1} at 1000^oC with activation energy for conduction of ~1.3eV. At lower temperatures, stabilized zirconias have conductivities that are many order of magnitude less than those of Na^+ and Ag^+ ion solid electrolytes

1.3 Conductivity measurements

1.3.1 D.C Methods

Measurements of accurate and meaningful conductivity values, especially in polycrystalline materials, are often quite difficult. Ideally, the d.c. conductivity should be measured in order to be sure that the values pertain to long range ion migration and not to dielectric losses such as would be associated with limited or localized rattling of ions within cages. The difficulty in making d.c. measurements is in finding an electrode material that is compatible with the solid electrolyte and that does not gives the polarization effects at the electrode –solid electrolyte interface. For example, if gold metal electrodes shown in Fig 1.6 are attached to a β-alumina crystal and a small voltage, e.g.100mV is applied across the crystal, Na^+ ions migrate preferentially towards the cathode, but pile up, without being discharged, at the gold/β-alumina interface. A Na^+ ion- deficient layer forms at the β-alumina/gold anode interface. The cell therefore behaves as a capacitor; a large instantaneous current I_0 is observed when the cell is switched on, whose magnitude is related to the applied voltage and the resistance of the β-alumina crystals, but the current then falls exponentially with time as shown in Fig. 1.6.

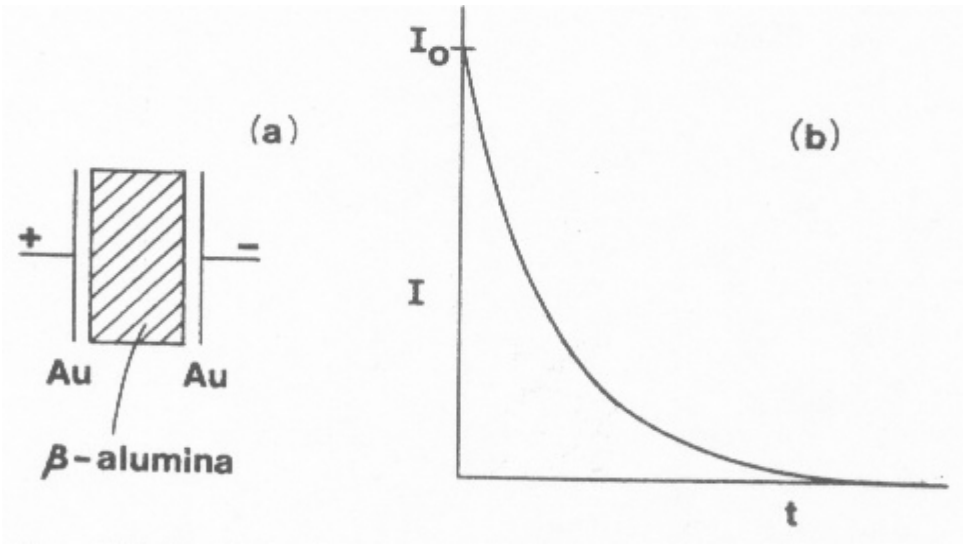

Figure 1.6: *Polarization at blocking electrodes in D.C measurements*

Interfacial problems in d.c. measurements may be overcome by using reversible electrodes i.e. electrodes that allow conduction by both electrons and mobile ions of the solid electrolyte. Using reversible electrodes, there is no polarization problem because Na^+ ions can move across the interface from electrode to solid electrolyte, and vice versa. Molten sodium is a suitable reversible electrode for β-alumina because the reaction occurs at sodium/β-alumina interface as given in equation (1).

$$Na^+ + e \leftrightarrow Na \qquad (1)$$

.

1.3.2 A.C. Methods

The alternative to d.c. conductivity measurements is to use a.c. methods and make measurements over a wide range of frequencies; d.c. conductivity values can usually be extracted from the a.c. data. In some cases it is possible to obtain information about electrode capacitance, grain boundary resistances, capacitances and the amount of electronic conductivity present.

A.C. measurements are often made with Wheatstone bridge type of apparatus shown in Fig 1.7 in which the resistance, R, and capacitance, C, of the sample are balanced against variable resistors and capacitors.

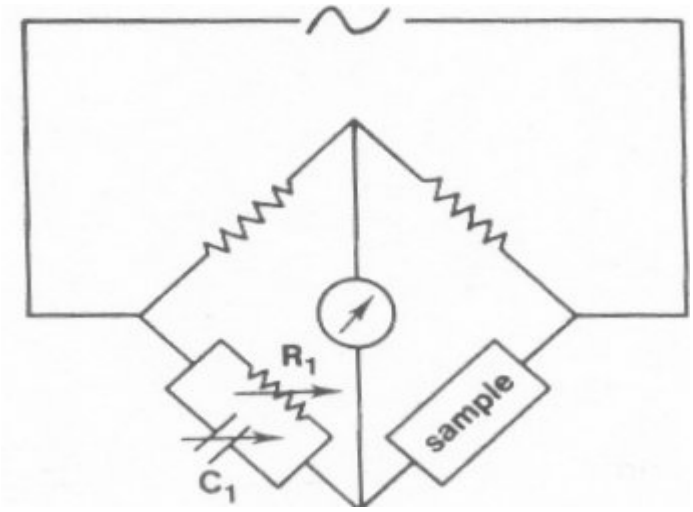

Figure 1.7: *Measurements of R and C with wheatstone bridge*

Many a.c. measurements are made with blocking gold electrodes. In these measurements no discharge or reaction occurs at the electrode-electrolyte interface. The gold-solid electrolyte interface may be represented as a double-layer capacitance, C_{dl}, with a typical magnitude of $1x10^{-6}Fcm^{-2}$. This double layer capacitance is effectively in series with the sample resistance. In a polycrystalline materials the overall sample resistance may be a combination of intragranular resistance or the bulk material resistance, R_b, and the intergranular or the grain boundary resistance , R_{gb}. Grain boundary resistances have an associated capacitance, C_{gb}, in parallel with R_{gb} whose magnitude depends inversely on the thickness of the grain boundary layer. For a parallel plate capacitor the capacitance, C, is given by $C = \varepsilon'\varepsilon_0 A d^{-1}$, where A is the area of the plates, d is their separation, ε_0 is the permittivity of the free space ($8.854x10^{-14}Fcm^{-1}$) and ε' is the dielectric constant or permittivity of the material between the plates. A typical value of C_{gb} is 10^{-9} F. It is more difficult to give a typical value for R_{gb}; usually the resistivity of grain boundary is larger than that of bulk crystal, but since the grain boundary layer may be several orders of magnitude thinner than the crystal dimensions, the actual grain boundary resistance, R_{gb}, may not necessarily be larger than R_b. Also, R_b and R_{gb} are usually highly temperature dependent where as capacitances change little with changing temperature. The bulk crystal resistance, R_b is in parallel with an associated bulk capacitance, C_b; C_b which corresponds to the bulk or

geometric capacitance pF the sample or cell and is related to the dielectric constant, ε', of the solid electrolyte, i.e.

$$\varepsilon' = C_b/C_0 \qquad (2)$$

where C_0 is the vacuum capacitance of the cell (the same electrode arrangement but with a vacuum between the electrodes).

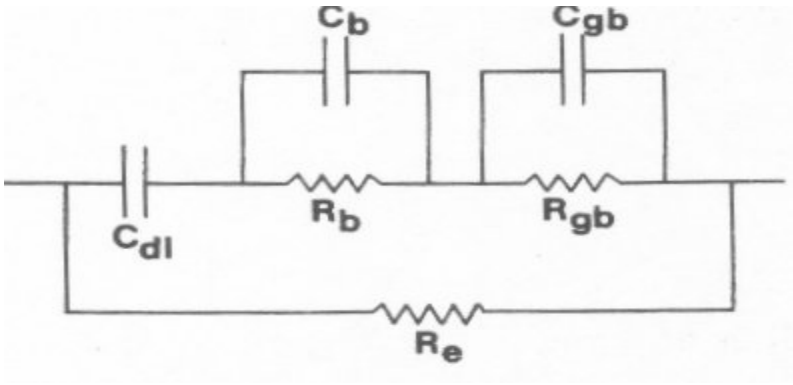

Figure1.8: *Equivalent circuit for a polycrystalline solid electrolyte:R_{gb}, C_{gb}-grain boundaries; R_b, C_b- bulk crystals; R_e- electronic resistance ; C_{dl}- electrode double- layer capacitance*

In solid electrolytes, the dielectric constant is the value which would occur in the absence of long range migration of ions; it can usually be observed experimentally in a.c. measurements if the frequency is sufficiently high so that the polarity of the applied voltage switches before the ions have enough time to move; ε' and C_b then correspond to the polarization of atoms and electrons, which occurs in normal dielectrics.

If solid electrolyte has an electronic conductivity as well as an ionic conductivity, this is represented by a separate resistance, R_e, in parallel with the rest of the equivalent circuit. If the electronic resistance is small enough in magnitude it can short-out the rest of the circuit including the double layer capacitance at the electrode-electrolyte interface that's why in most solid electrolytes, $R_e >> (R_{gb}+R_b)$ and R_e can effectively be ignored.

1.4 Applications of solid electrolytes

1.4.1 Electrochemical cell- principles

Electrochemical cells are of two types: power cells and sensors. In an ideal power cell, the ionic current through the electrolyte inside the cell matches an electronic current through an external load. A solid electrolyte acts as a separator of the two electrodes as well as a carrier of the internal ionic current. It is in the form of a membrane of thickness L and area A that separates electronically the two electrodes of the cell. Any internal electronic current across the electrolyte reduces the power output. The internal resistance to the ionic current is

$$R_i = L/\sigma_i A \quad (3)$$

where, σ_i is the ionic conductivity of the electrolyte. For a current I through the cell, the voltage IR_i represents a potential drop that is to be minimized. Even in potentiometric sensors, the resistance R_i must be maintained below a certain level to obtain satisfactory sensitivity and speed of response, and any electronic contribution to the internal cell current must be factored into the cell calibration.

These simple considerations lead to the following general quality criteria for a solid-electrolyte material to be used in an electrochemical cell.

1.To minimize R_i for a given intrinsicσ_i , the material must lend itself to easy fabrication into a mechanically strong membrane of small L and large A. Optimization of cell design may also require the fabrication of membranes of complex shape.

2. Unless an exceptionally small L/A ratio is feasible, a R_i acceptable generally requires a $\sigma_i > 10^{-2}$ Scm^{-1} at the cell operating temperature T_{op}. In general, the conductivity is a tensor, but in polycrystalline electrolytes is a scalar quantity.

3. A transport number

$$t_i = \sigma_i/\sigma = 1 \text{ where } \sigma = \sum_j \sigma_j + \sigma_e \quad (4)$$

is needed. In general, there is only one mobile ion in a solid electrolyte so that $\sum_j \sigma_j = \sigma_i$. Because any electronic mobility is much greater than the ionic mobility and relatively small number of electronic carriers can make the electronic conductivity σ_e competitive with σ_i , *i.e.* $\sigma_e \geq \sigma_i$**,** to degrade t_i to an unacceptable level.

4. The resistance to ion transfer across the reactant/electrolyte interface must be low.

5. Chemical stability in the working environment requires that the electrolyte is neither reduced by the reductant at the negative electrode nor oxidized by the oxidant at the positive electrode. Thermodynamic stability is only achieved by placing the bottom of the solid-electrolyte conduction band above the highest occupied molecular orbital (HOMO) of the

reductant and the top of the solid-electrolyte valence band below the lowest unoccupied molecular orbital (LUMO) of the oxidant as illustrated in Fig 1.9. Where the reactants are the metallic electrodes, as in a storage battery, the energies of the HOMO and/or LUMO are given by the Fermi energy of the anode and/or cathode.

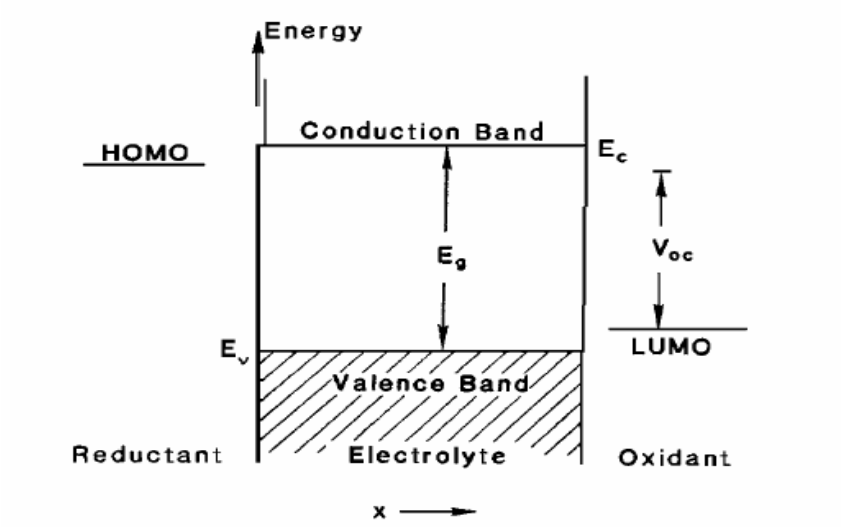

Figure 1.9: *Placement of reactant energies relative to the edges of the electrolyte conduction and valence bands in a thermodynamically stable electrochemical cell at flat band potential*

6. The mobile ion of a solid electrolyte must be the working ion of the cell.

7. The cost of material and fabrication is always a consideration.

Consider a schematic cell shown in Fig.1.10 which contains a solid electrolyte membrane separating two electrode compartments. The latter may contain solid liquid or gasses. There may be similar or dissimilar materials in both, e.g. oxygen gas at two different pressures or the two components of a cell, e.g. sodium and sulphur.

The e.m.f. of a cell reaction is given by the Nernst equation:

$$E=E_0+RT/nF \log_e [O_x]/[Red] \qquad (5)$$

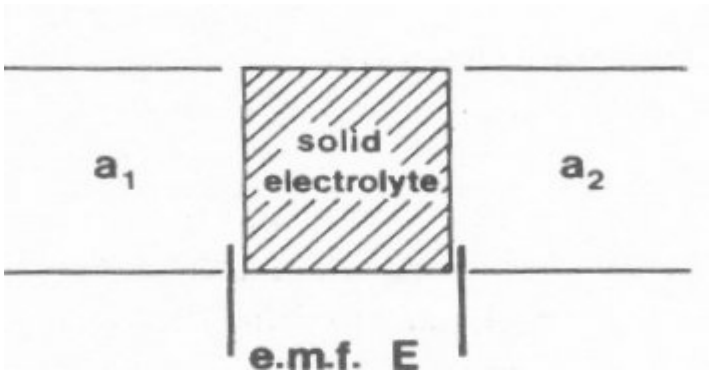

Figure1.10: *Electrochemical cell containing solid electrolyte*

Two such equations are usually needed, one for the reaction occurring at each electrode. Suppose that at the anode the following oxidation reaction occurs:

$$M \rightarrow M^{+} + e$$

Then

$$E_1 = E_{OM/M^{+}} + RT/F \log_e [M^{+}]/[M] \quad (6)$$

In which $E_{OM/M^{+}}$ is the standard redox potential for that reaction. $[M^{+}]$ and [M] are the concentrations of the two species and F is the faraday unit, 96500 Coulombs. The M^{+} ions that are generated at the anode diffuse through the solid electrolyte and react at the cathode with X^{-}, produced according to

$$X + e \rightarrow X^{-}$$

for which

$$E_2 = E_{O\,X^{-}X} + RT/F \log_e [X]/[X^{-}] \quad (7)$$

Summation of E_1 and E_2 gives the overall e.m.f. for the reaction: M+X→ MX, and this is related to the free energy of formation of MX by

$$\Delta G = -nEF \quad (8)$$

1.4.2 Batteries

Much of the impetus for research on solid electrolytes has come from their possible use in new types of battery. The sodium-sulphur cell utilizes Na^{+} β-alumina solid electrolyte and is probably the most important one. It is a high density battery, i.e. it has a high energy/power to mass ratio and is undergoing extensive development and testing in several countries for use in, for example, electric cars and for power station load leveling. Basically, it consists of a molten sodium anode and a molten sulphur cathode separated by β-alumina solid

electrolyte. Usually, the β-alumina is fabricated in the form of a tube closed at one end with the sodium inside and the sulphur outside (or vice versa). Since molten sulphur is a covalently bonded solid it is a non-conductor of electricity and the cathode material that is used consists of graphite felt impregnated with sulphur. The outer casting of the cell is made of stainless steel and serves as a current collector as shown in Fig. 1.11. The cell discharge reaction is:

$$2Na + xS \rightarrow Na_2S_x \qquad (9)$$

where x depends on the level of charge in the cell. In the early stages of discharge, x is usually given as five, which corresponds to the formula of most sulphur – rich sodium sulphide, Na_2S_5, because x decreases as discharge continues.

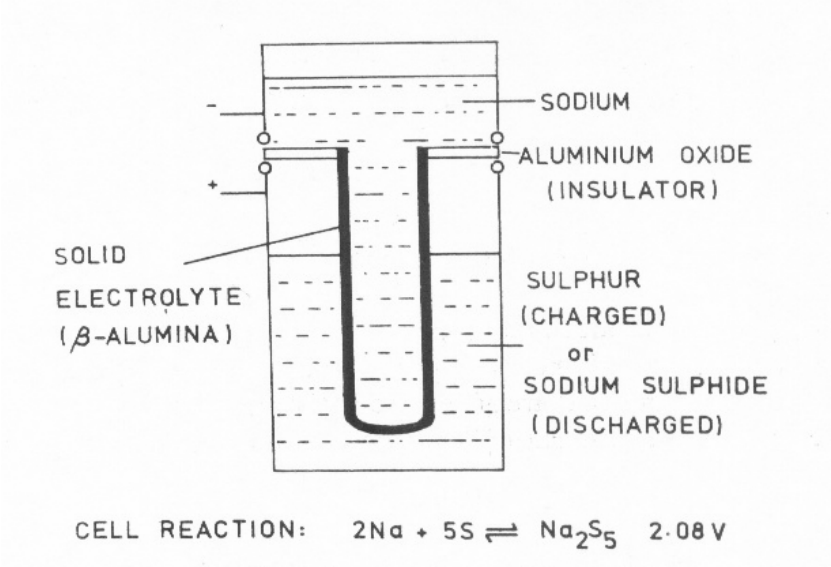

Figure 1.11: *The sodium-sulphur cell*

The phase diagram for the sodium sulphur system is shown in Fig.1.12. The sodium sulphur cell operates at 300 to 350^{o}C, which is the lowest temperature at which the discharge products are molten for a large range of compositions. From the phase diagram it can be seen that when discharge reaches the stage at which $x \leq 3$ (i.e.60%S, 40%Na), the liquid rises rapidly and the crystalline Na_2S_2 begins to form; further discharge would lead to a gradual freezing of the cathode material. The open circuit voltage of the cell depends on both the level of charge and temperature. The maximum open circuit voltage for a fully charged cell is 2.08V at 300^{o}C. This decreases on discharge to ~ 1.8V for x = 3.

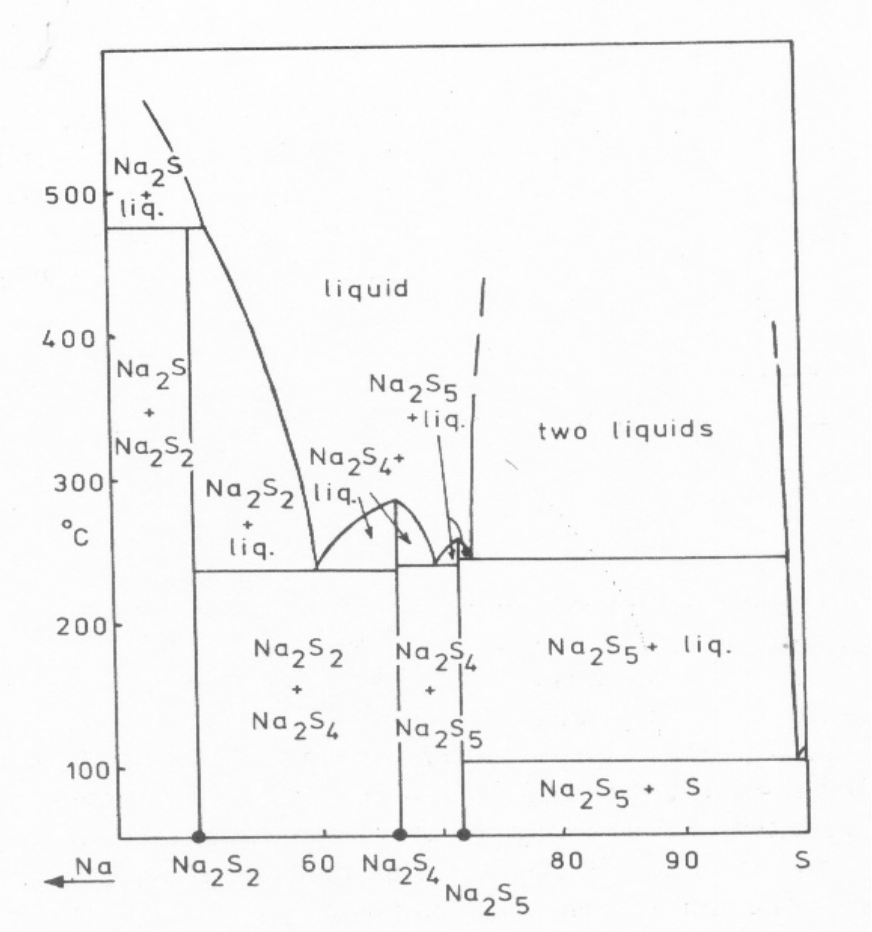

Figure 1.12: *Phase diagram for the sodium sulphur system*

Other types of cells that are finding applications are miniature primary cell which operates at room temperature and which have a long life rather than a high power output. They are used in electronic watches, heart pacemakers and in military applications.

1.4.3 Oxygen concentration cells and sensors

Electrochemical cells containing solid electrolytes may be used for the measurement of partial pressures of gases or the concentration of gases dissolved in liquids. An oxygen concentration cell that utilizes a stabilized zirconia solid electrolyte in the form of an open ended tube is shown in Fig.1.13

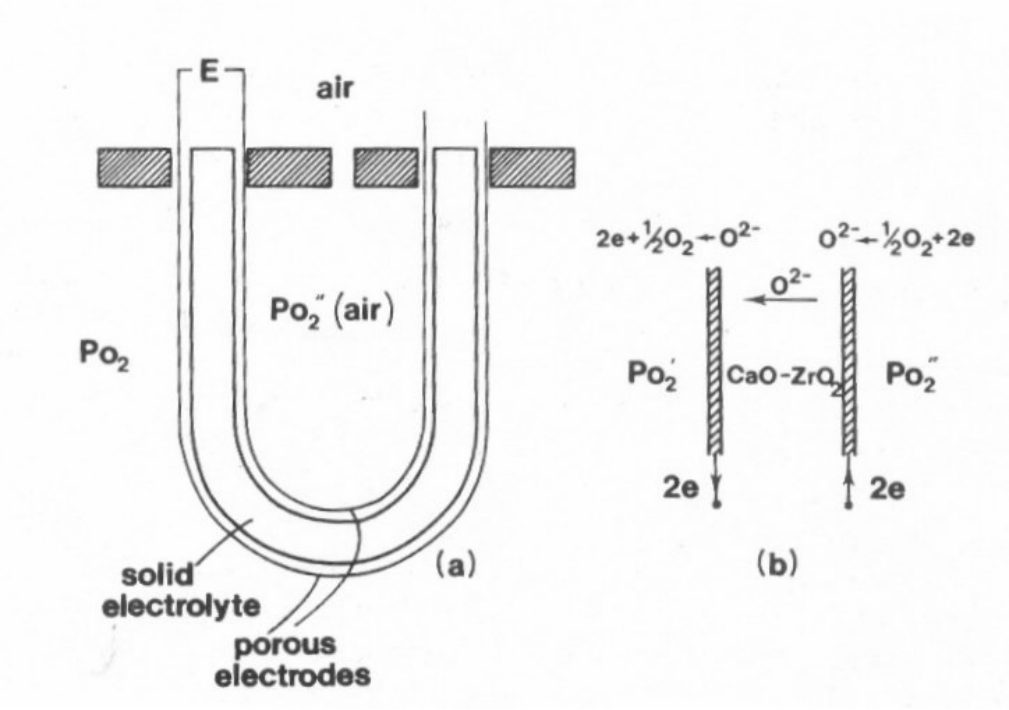

Figure1.13: *Oxygen concentration cell with stabilized zirconia electrolyte*

Inside the tube, a reference gas such as air is used. The tube is coated with porous metal electrodes to allow absorption and liberation of oxygen gas. If the partial pressure of oxygen that is to be measured, P'_{O2}, is less than the reference pressure, P''_{O2}, the electrode reaction shown in figure 1.13 (b) take place and oxide ions migrate through the solid electrolyte from right to left. The Nernst equations for the reactions at each electrode may be combined into a single equation that relates the difference in oxygen partial pressures to the cell voltage, i.e.

$$E = RT/4F \log_e (P''_{O2}/ P'_{O2}) \qquad (10)$$

The cell operates at temperature between ~500 and 1000^oC (in order that transport of O^{2-} ions through the electrolyte occurs sufficiently rapidly) and can be used to measure oxygen partial pressure as low as 10^{-16} atm. At lower pressures the zirconia becomes an electronic conductor and the cell shortcircuits. Oxygen concentrations cell such as zirconia probe have various uses, e.g. the analysis of exhaust gases and pollution, measurement of the consumption of oxygen gas during respiration and study of equilibria such as CO/CO_2,

H_2/H_2O and metal/metal oxide. They may also be used to probe the oxygen activity in molten metals, e.g. steel, by dipping the probe into the melt. Oxygen concentrations are measured from a calibrated meter and the response of the probe is usually very rapid.

1.4.4 Fuel cells

Stabilized zirconia is used in either tube or disc form as a solid electrolyte in fuel cells. The two electrode compartments contain (a) air or O_2 and (b) a fuel gas, e.g. H_2, CO. The zirconia is again coated with porous metal electrodes and the cell reaction takes place as follows:

$$H_2 + 1/2\ O_2 \rightarrow H_2O \quad \text{or } CO + 1/2O_2 \rightarrow CO_2 \tag{11}$$

The advantages of this type of fuel cell are minimum electrode polarization problems and high current densities, e.g. $0.5Acm^{-2}$. However, designing difficulties sometimes are due to various reasons.

The fuel cell can also be used as an electrolyser and as a means of storing energy by reversing the direction of current flow. Thus, steam can be decomposed as H_2 and O_2 which can be stored. It could also be used to regenerate oxygen from CO_2 in spaceships and to deoxidize liquid metals.

CHAPTER 2

TYPES OF FUEL CELL AND ELECTROLYTE

2.1 Fuel Cell

The modern scientific and technological approach in the area of energy production is to develop inexpensive devices, which could satisfy the current drive for cleaner and more efficiently distributed power, particularly in combined heat and power systems. In this context fuel cells represent a promising and viable alternative for large scale generation of electricity, with minimal undesirable chemical, thermal and acoustic emissions. A fuel cell is a device that directly converts the chemical energy of reactants (a fuel such as hydrogen, natural gas, methane or methanol, and an oxidant air or oxygen), into electricity. Fuel cells are often classified according to the kind of electrolyte they incorporate and also the temperature range of their operation. A schematic representation of fuel cell with anode and cathode electrodes separated by electrolytes is shown in Figure 2.1

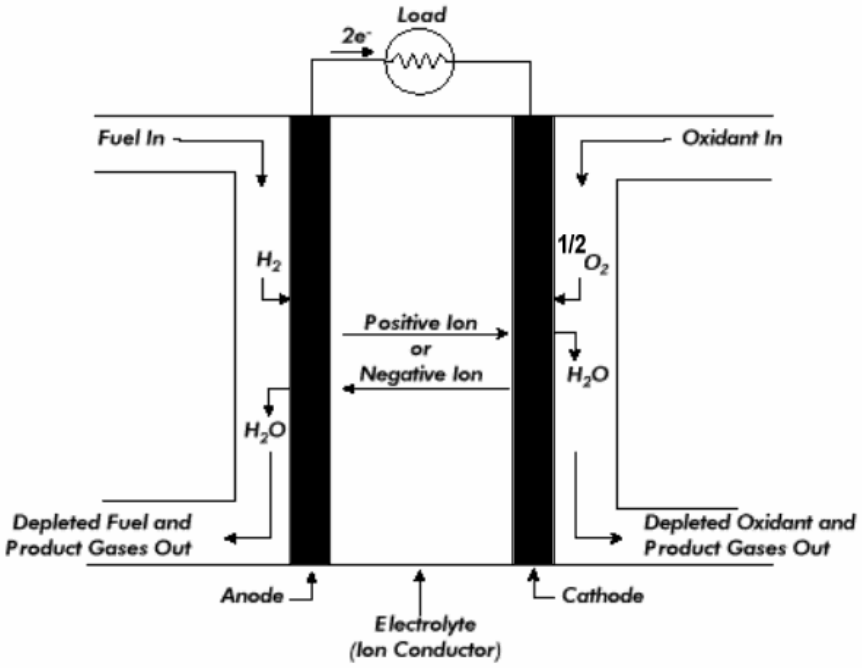

Figure 2.1: *Schematic representation of Fuel Cell (SOFC)*

The principles of fuel cell operation were first reported by Sir William Robert Grove in 1839 [3]. In that Fuel cell dilute sulphuric acid was used as an electrolyte and operated at room temperature. Ceramic fuel cells came into existence much later and began with Nernest's discovery of solid-oxide electrolytes in 1899 [4] and the operation of the first ceramic fuel cell at a temperature of 1000^{o}C was demonstrated by Baur and Pries in 1937 [5].

In their experiment they used zirconium, yttrium, cerium, lanthanum and tungsten as electrolytes, little success. Much of the research, however, was short-lived as melting, short-circuiting, and high electrical resistance inside the cell materials created numerous technical hurdles. Their designs were not as good to provide electrical conductivity upto the mark as was expected due to unwanted chemical reactions between the electrolytes and various gases, including carbon monoxide.
By the late 1950's, research into solid oxide technology began to accelerate because of advancement in ceramic processing.

2.2 Types of Fuel Cells

The category of fuel cells are generally characterized by electrolyte material utilized within these devices. The electrolyte is a substance between the anode and the cathode, serving as the bridge for the ion exchange that generates electrical current. There are six types of fuel cells that are significantly different from each other in many respects; however, the key distinguishing feature is the electrolyte material. These fuel cells are as follows;

(1)Phosphoric Acid Fuel Cell (PAFC)

(2)Alkaline Fuel Cell (AFC)

(3)Proton Exchange Membrane Fuel Cell (PEMFC)

(4)Direct Methanol Fuel Cell (DMFC)

(5)Molten Carbonate Fuel Cell (MCFC)

(6)Solid Oxide Fuel Cell (SOFC)

2.2.1 Phosphoric Acid Fuel Cell (PAFC)

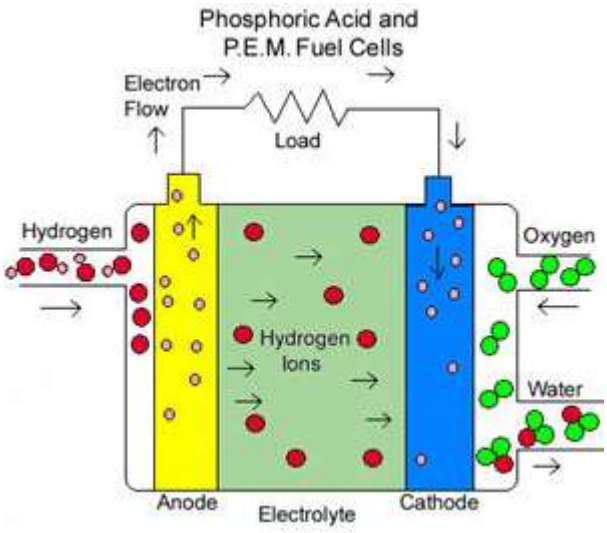

Figure 2.2: *Diagrammatic Representation of Phosphoric Acid Fuel Cell*

PAFCs as shown in Fig. 2.2 generate electricity at more than 40% efficiency -- and nearly 85% of the steam this fuel cell produces is used for cogeneration -- this compares to about 35% for the utility power grid in the United States. Operating temperatures are in the range of 150 - 200^{o}C. At lower temperatures, phosphoric acid is a poor ionic conductor, and carbon monoxide (CO) poisoning of the Platinum (Pt) electro-catalyst in the anode becomes severe. The electrolyte is liquid phosphoric acid soaked in a matrix. One of the main advantages to this type of fuel cell, besides the nearly 85% [6] cogeneration efficiency, is that it can use impure hydrogen as fuel. Disadvantages of PAFCs include: it uses expensive platinum as a catalyst, it generates low current and power comparably to other types of fuel cells, and it generally has a large size and weight. PAFCs, however, are the most mature fuel cell technology.

2.2.2 Alkaline Fuel Cell (AFC)

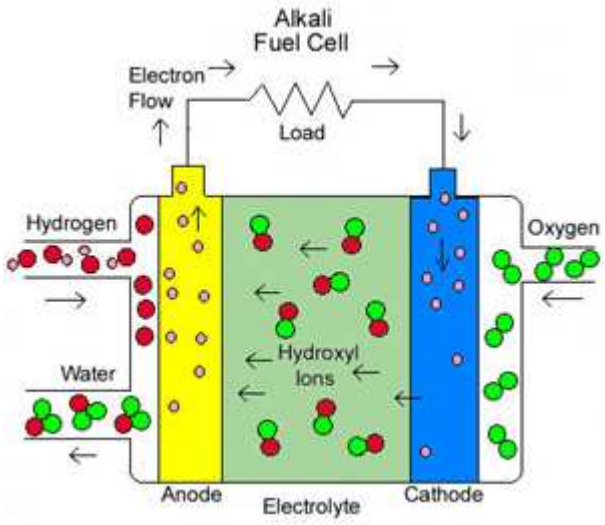

Figure 2.3: *Diagrammatic Representation of Alkaline Fuel Cell*

Long used by NASA on space missions, these cells can achieve power generating efficiencies of up to 70 percent. They were used on the Apollo spacecraft to provide both electricity and drinking water. Their operating temperature is 150 to 200^{o}C [6]. They use an aqueous solution of alkaline potassium hydroxide soaked in a matrix as the electrolyte. This is advantageous because the cathode reaction is faster in the alkaline electrolyte, which means higher performance. Until recently they were too costly for commercial applications. They typically have a cell output from 300 watts to 5 kW.

2.2.3 Proton Exchange Membrane Fuel Cell (PEM)

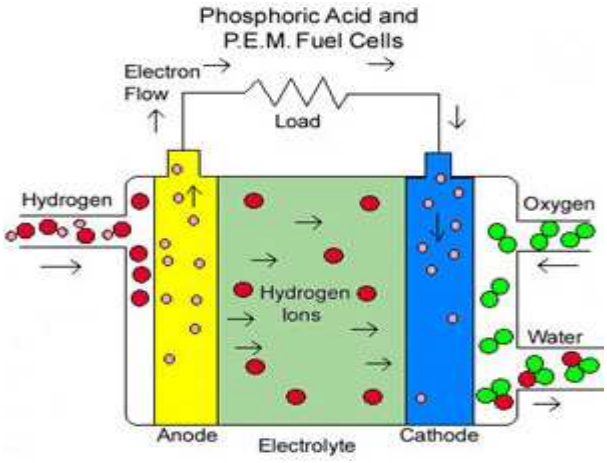

Figure 2.4: *Diagrammatic Representation of PEM*

These cells operate at relatively low temperatures about 80^{o}C [6], have high power density, can vary their output quickly to meet shifts in power demand, and are suited for various applications, such as in automobiles due to quick startup is required. The proton exchange membrane is a thin plastic sheet that allows hydrogen ions to pass through it. The membrane is coated on both sides with highly dispersed metal alloy particles (mostly platinum) that are active catalysts. The electrolyte used is a solid organic polymer poly-perflourosulfonic acid. The solid electrolyte is an advantage because it reduces corrosion and management problems. Hydrogen is fed to the anode side of the fuel cell where the catalyst encourages the hydrogen atoms to release electrons and become hydrogen ions (protons). The electrons travel in the form of an electric current that can be utilized before it returns to the cathode side of the fuel cell where oxygen has been fed. At the same time, the protons diffuse through the membrane (electrolyte) to the cathode, where the hydrogen atom is recombined and reacted with oxygen to produce water, thus completing the overall process. This type of fuel cell is, however, sensitive to fuel impurities. Cell outputs generally range from 50 to 250 kW.

2.2.4 Direct Methanol Fuel Cells (DMFC)

These cells are similar to the PEM cells in that they both use a polymer membrane as the electrolyte. However, in the DMFC, the anode catalyst itself draws the hydrogen from the liquid methanol, eliminating the need for a fuel reformer. Efficiencies of about 40% are expected with this type of fuel cell, which would typically operate at a temperature between

50 -100 ^{o}C. This is a relatively low range, making this fuel cell attractive for tiny to mid-sized applications, to power cellular phones and laptops. Higher efficiencies are achieved at higher temperatures. A major problem, however, is fuel crossing over from the anode to the cathode without producing electricity.

2.2.5 Molten Carbonate Fuel Cell (MCFC)

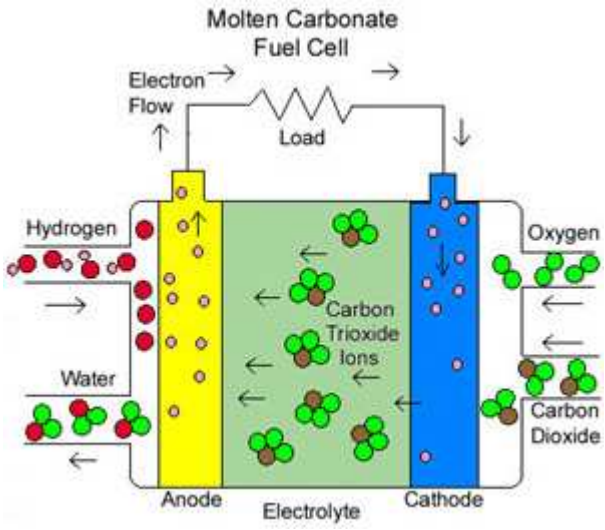

Figure 2.5: *Diagrammatic Representation of MCFC*

These fuel cells use a liquid solution of lithium, sodium and/or potassium carbonates, soaked in a matrix for an electrolyte. They promise high fuel-to-electricity efficiencies, about 60% normally or 85% with cogeneration, and operate at about 650^{o}C [6]. The high operating temperature is needed to achieve sufficient conductivity of the electrolyte. Because of this

high temperature, noble metal catalysts are not required for the cell's electrochemical oxidation and reduction processes. The high operating temperature serves as a big advantage because this implies higher efficiency and the flexibility to use more types of fuels and inexpensive catalysts as the reactions involving breaking of carbon bonds in larger hydrocarbon fuels occur much faster as the temperature is increased. A disadvantage to this, however, is that high temperatures enhance corrosion and the breakdown of cell components.

2.2.6 Solid Oxide Fuel Cell (SOFC)

Solid oxide fuel cell is another highly promising fuel cell; this type could be used in high-power applications including industrial and large-scale central electricity generating stations. Some developers also see SOFC use in motor vehicles and are developing fuel cell auxiliary power units (APUs) with SOFCs.

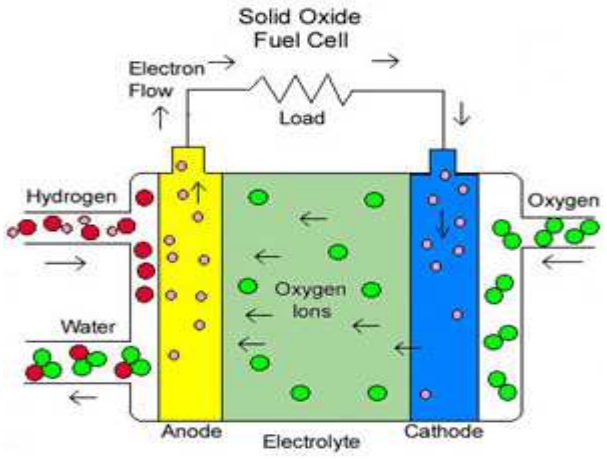

Figure 2.6: *Diagrammatic Representation of SOFC*

In solid oxide fuel system a hard ceramic material such as of solid zirconium oxide and a small amount of ytrria is used instead of a liquid electrolyte, allowing operating temperatures to reach 1000^{o}C. Power generating efficiencies could reach 60% and 85% with cogeneration and cell output is up to 100 kW. One type of SOFC uses an array of meter-long tubes (tubular design), and other variations include a compressed disc planar design. Tubular SOFC designs are closer to commercialization and are being produced by several companies around the world.

2.3 ADVANTAGES OF SOFCs

Among the initially developed devices, the widely used ones are the low temperature phosphoric acid fuel cells [8] and those based on aqueous alkaline electrolytes [9]. However the aqueous electrolytes may flood the porous electrodes, evaporate, undergo compositional changes, decompose and eventually lead to poor performance. Attempts to overcome some or all of these shortcomings would result in a rather complex design. Moreover, because of the relatively low temperature of operation restrains the kinetics, expensive platinum based catalysts are used at the electrolyte-electrode interface.

The fuel cell operating at elevated temperatures (~700^{o}C or above) employ either a mixed molten carbonate or ceramic solid oxide as the electrolyte and accordingly known as the molten carbonate fuel cells (MCFCs) and the solid oxide fuel cells (SOFCs), respectively. Both these devices can use hydrocarbon fuels, reformed internally on the electrodes, with ordinary air as the oxidant; both are having a comparable efficiencies, which are higher than those of carnot heat engines, and both are cool enough to prevent NO_x formation [10]. The main distinction between the two cells, however, lies in the choice of electrolyte. A system having molten salt as the working medium is more prone to creep and corrosion than metals and ceramics. On the other hand, a ceramic-based system is subjected to the risk of thermal shock and undesirable gas permeation. SOFCs have an edge over MCFCs in that they allow the fuel cells to run at higher temperatures expensive precious metal catalysts are not needed to promote the reaction between hydrogen and oxygen. Methane is readily reformed into hydrogen and carbon monoxide. The waste heat from the cell is useful in powering heaters, boilers and air conditioners. It is interesting to note that at the upper end of its temperature range, unlike the MCFC, SOFC is an all ceramic system, which signifies the prospect of miniaturization of the device without sacrificing the efficiency. Miniaturization principally stems from the availability of the well developed techniques of thick- and thin- film technology. Another advantage of SOFC over the MCFC is that there is a problem of electrolyte migration in MCFC while no such problem exists in the SOFCs. Further the kinetics of present day SOFCs are faster than their molten carbonate counterparts.

2.4 Properties required for SOFC Electrolytes:

The electrolyte for solid oxide fuel cell must be stable in both reducing and oxidizing environments and must have sufficiently high ionic with low electronic conductivity at cell operating temperature. In addition the material must be able to be formed into a thin strong film with no gas leaks. The required properties for these materials, fixed by both electrochemical constraints and high operating temperature, are the following:

- High ionic conductivity($\geq 0.1 Scm^{-1}$ at 900^0C)
- Low electronic transference number(<10-3 at 900^0C)
- Phase stability from room temperature to 1100^0C approximately.
- Thermal expansion characteristics compatible with other cell components.
- Chemical compatibility with electrode and interconnection materials and with oxygen and fuel gas as well.
- Gas tightness
- Fracture toughness(>400MPa at room temperature)
- Moderate cost of materials and fabrication.

2.5 Various electrolyte materials for SOFCs

Although there are several candidate oxide-ion electrolytes, none is completely satisfactory for SOFCs with operating temperature below 800^oC. They fall into a few structural categories, but in each, oxide-ion conduction is by oxygen vacancies. The different problems encountered with these candidates produces challenges for the designer of an oxide-ion electrolyte [2].

2.5.1 Yttria Stabilized Zirconia

The material used as the solid electrolyte in most of the fuel cells is Yttria-stabilized zirconia (YSZ), because of its higher conductivity and desirable stability in both oxidizing and reducing atmospheres. High-temperature zirconia (ZrO_2) has the cubic fluorite structure as given in Fig. 2.7. On cooling from its melting point (2680^oC), it transforms to a tetragonal form at 2370^oC and then to a monoclinic form at 1170^oC [7]. The high-temperature structure can be stabilized to room temperature by substitution of larger cations of lower valence (e.g., $Zr_{1-x}Ca_xO_{2-x}$ or $Zr_{1-x}\ Y_xO_{2-0.5x}$) for Zr^{4+}, which also introduces oxygen vacancies on the normal sites and therefore oxide-ion conductivity. If the dopant content is not sufficient to

fully stabilize the cubic structure, then the material may consist of two or more phases. The amount of dopant required to fully stabilize the cubic structure is about 12–13 mol% for CaO, 8–9 mol% for Y_2O_3 and Sc_2O_3, and 8–12 mol% for other rare-earth oxides [7].

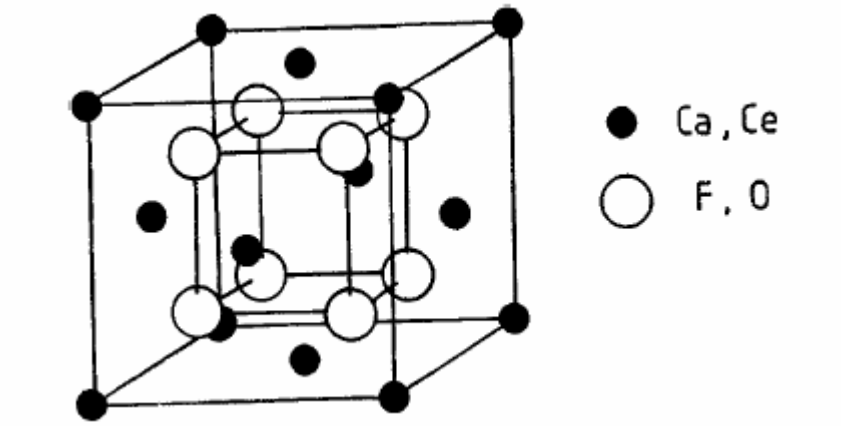

Figure 2.7: *The cubic fluorite structure of CaF_2 or CeO_2*

The oxygen vacancy concentration gives rise to high oxygen-ion mobility. Oxygen ion conduction takes place in stabilized ZrO_2 by the movement of oxygen ions via vacancies. Over a wide range of temperature, the ionic conductivity of stabilized ZrO_2 is independent of oxygen partial pressure over several orders of magnitude. Under these conditions, the ionic transport number is very close to unity (i.e. limited electronic conduction).

The tetragonal phase is stabilized with low-dopant content, i.e., about 2 to 2.5 mol% for Y_2O_3 and several other rare-earth oxides. The cubic phase has low strength, toughness, and thermal shock resistance, whereas the tetragonal phase has extremely high strength and toughness due to a stress-induced phase transformation to monoclinic zirconia. Metastable tetragonal zirconia polycrystals (TZP) have been shown to exhibit ionic conductivity higher than YSZ below 400^{o}C and are poor electronic conductors [11]. Yttria-doped tetragonal zirconia has been tested as a component of a composite electrolyte with 20% Al_2O_3. Addition of the insulating phase has been found to enhance the conductivity. Alumina is believed to act as a scavenger of the glassy phase that is usually encountered at the grain boundaries in pure TZP; this glassy phase hinders the transport of ions at the grain boundaries.

Stabilized zirconia, however, requires an operating temperature of ~ 1000^{o}C due to conductivity requirements. Various problems are associated with such a high temperature: thermal stresses at the electrolyte-electrode and electrode-interconnect interfaces, interdiffusion between electrodes and electrolyte and degradation of the electrodes due to demixing. A substantial effort has has been made to develop electrolytes, alternative to stabilized zirconia, with higher ionic conductivity at lower temperatures. Lowering the temperature would also extend the operating life of fuel cells and ensure a shorter heating time before the start up. With this aspect in view quest for the development of new electrolytes has been revitalized.

2.5.2 Ceria Doped Alkaline earth oxides

Several studies have shown that ceria (CeO_2) doped with alkaline- earth or rare- earth oxides exhibits ionic conductivity up to two orders of magnitude higher than zirconia at comparable temperatures. Ceria has the same fluorite structure as thoria and doped zirconia, but is different in that pure CeO_2 undergoes large departures from stoichiometry at elevated temperatures, leading to appreciable electronic conduction, which is undesirable. Yahiro *etal*. [12] overcame this problem by coating the CeO_2 – based electrolyte with a film (~1μm) of YSZ. The resulting "composite solid electrolyte" exhibit high ionic transport number, an output voltage close to the theoretical value, and higher conductivity than a single phase YSZ in the temperature range 600-800^{o}C.

2.5.3 Perovskite Structured Materials

Development of other materials, especially those possessing sufficient ionic conductivities at intermediate temperatures (600 - 800^{o}C), has received much interest recently. A replacement of YSZ by a reduced – temperature oxygen ion conductor in SOFCs would greatly reduce material and fabrication problems and improve cell reliability during prolonged operation. In this connection several doped perovskite (ABO_3) such as $DyAlO_3$, $CaAl_{0.7}TI_{0.3}O_3$, $BaCe_{0.9}Gd_{0.1}O_3$ and $SrZr_{0.9}Sc_{0.1}O_3$ etc., solid electrolytes have been identified [13]. However, several of these materials (most of which are protonic conductors) do not possess long-term

phase stability as manifested in unsteady operating potential as result of ageing under intermediate-temperature fuel cell conditions [14].

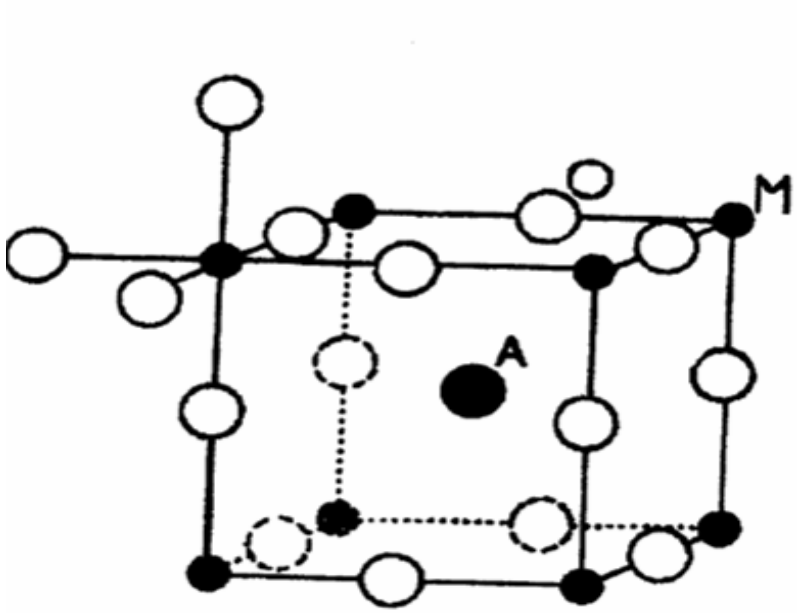

Figure 2.8: *Cubic perovskite*

In SOFCs hydrogen like protonic conductors could also be used as the fuel. Iwahara *et al*. [15] have found that the perovskite-type oxides based on $SrCeO_3$ and $BaCeO_3$ with partial substitution of Ce^{+4} by some of the rare earth ions (Ln^{3+}) are excellent high temperature proton conductors .

Yet another promising material is bismuth based oxides. Stabilized bismuth oxide (Bi_2O_3) exhibits the highest ionic conductivity at comparable temperatures. This greater ionic conductivity of stabilized Bi offers the possibility of its use as an electrolyte in SOFCs operation at lower temperatures (<1000^oC).

2.5.4 Bismuth oxide based electrolytes

Pure bismuth oxide has two thermodynamically stable crystallographic polymorphs. One is α-Bi_2O_3, which is stable below 730^oC and has a monoclinic structure, which allows p-type conduction. The other is δ-Bi_2O_3, which is stable above 730^oC, up to its melting temperature of 825^oC, and crystallizes in the fluorite structure (cubic CaF_2) structure. In addition to these phases, tetragonal (β-Bi_2O_3) and body centered cubic (γ-Bi_2O_3) crystallographic modifications are also known to exist below 650^oC, as metastable phases [16].

The δ-Bi_2O_3 contains 25% of the anion sites (one oxygen site per formula) vacant, and as a result exhibits very high O^{2-} ion conductivity (~1 S cm^{-1} near the melting point). The conductivity is upto two orders of magnitude greater than in the stabilized zirconia. The high polarizability of the Bi^{3+} ion with its lone pair of electrons has been viewed as its conductivity enhancing factor. Another possibility could be the existence of a weaker metal-oxygen bond between bismuth and oxygen as compared to that between zirconium and oxygen this might promote a greater mobility of the vacancies in the lattice.

However the high conductivity phase is stable over a very narrow range of temperature (730- 800^oC). Further the volume change associated with the δ→α phase transition leads to cracking and severe deterioration of the material. Thus for application of Bi_2O_3 as a solid electrolyte in fuel cells, it is imperative that the high temperature cubic phase is stabilized. The temperature dependence of conductivity of various solid electrolytes shows that Bi_2O_3 based material stand out as superior oxide electrolytes. However, the main drawback of this material is its small potential range of its ionic conduction. Bi_2O_3 is also prone to reduction into metallic bismuth, even at moderately low oxygen partial pressure.

A large number of studies have shown that the high conductivity δ-phase in Bi_2O_3 could be stabilized at lower temperatures, by the addition of dopants [41]. However, doping (by various di-, tri-, tetra-, penta- or hexavalent cations) also lowers the ionic conductivity. In some cases, doping leads to transformation into a more conducting rhombohedral phase which, however, undergoes decomposition which lead to decrease in ionic conductivity below 700^oC temperature. The extent and nature of the phase structure of the doped Bi_2O_3 (i.e. fcc or rhombohedral or a mixture of both), depends on the ionic radii of the dopants, their proportion in the host material and thermal history.

2.5.4.1 Bi_2O_3 - M_2O_5 (M= V, Nb, Ta) system

A number of phase equilibria and electrical conductivity investigations have been carried out in the Bi_2O_3- M_2O_5 systems. Recently, Abraham *etal.*[36] predicted high ionic conduction in the $Bi_4V_2O_{11}$ system ($2Bi_2O_3$ - V_2O_5). This compound has a layered structure and undergoes several structural transitions between 405^oC and congruent melting point, 887^oC. Bismuth vanadate $Bi_4V_2O_{11}$, is the parent compound of an extensive range of substitutional solid

solutions which have become known as the BIMEVOX family. $Bi_4V_2O_{11}$ shows complex polymorphism but essentially has three main polymorphs $\alpha \rightarrow \beta$ (447^oC) and $\beta \rightarrow \gamma$ (567^oC). Substitution of V by a host of iso- and alio-valent cations leads to the stabilization of the highly conducting γ-polymorph to room temperature. Conductivities in the order of 10^{-1} S cm^{-1} have been reported at 600^oC for the parent compound and a number of the substituted BIMEVOX. This behavior is believed to be combined result of a high concentration of anion vacancies and a disordering of the anion vacancies within the structure. At low temperatures the $Bi_4V_2O_{11}$ structure (α and β phases) becomes more ordered, the unit cells larger, and the conductivity markedly lower. The low temperature conductivity can be enhanced by stabilizing the disordered γ phase at room temperature, which can be achieved by the partial substitution of various metallic ions for vanadium and bismuth sites.

Bismuth vanadate is a ferroelectric material with an aurivillius type structure consisting of $(Bi_2O_2)^{2+}$ layers interleaved with perovskite-like sheets of $(VO_{3.5})^{2-}$ as shown in Fig 2.9.The idealized structure of $Bi_4V_2O_{11}$ consists of alternating layers of $[Bi_2O_3]_n^{2n+}$ and $[VO_{3.5}\square_{o.5}]_n^{2n+}$, where □ represents oxide ion vacancies. The $[Bi_2O_2]_n^{2n+}$ layers have basal edge-shared BiO_4 square pyramidal groups with the oxygen atoms forming the basal plane and the bismuth in the apical position. The vanadate layer in the idealized structure is made up of VO_6 octahedra which corner share in the equatorial plane. This layer is distorted in the real structure of α- $Bi_4V_2O_{11}$.In addition distortion of the apical positions yields a structure in which majority of sites are in fact distorted tetrahedral. In the structure determination of α-$SBi_4V_2O_{11}$ both tetrahedral and octahedral V coordinatins were found [17].

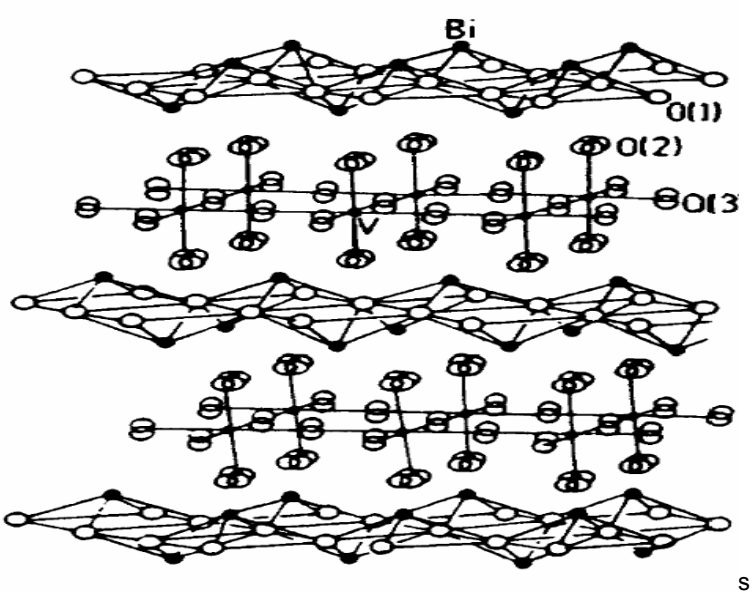

Figure 2.9: *The Structure of Bismuth Vanadate*

The relationship of the three major polymorphs in $Bi_4V_2O_{11}$ can be explained with reference to mean orthorhombic cell $a_m \approx 5.53$, $b_m \approx 5.61$, $c_m \approx 15.28$ A^o ,for the γ- phase $a = b \approx a_m/\sqrt{2}$,$c \approx c_m$;for the β- phase $a_m \approx 2\ a_m$, $b_m \approx b_m$, $c_m \approx c_m$; for the α-phase $a_m \approx 3a_m$, $b_m \approx b_m$, $c_m \approx c_m$. The true crystal system of the α-phase however has been the subject of some discussion. It has been found [17] that low levels of cationic impurities present in the commercial samples of V_2O_5 result in an orthorhombic phase for α- $Bi_4V_2O_{11}$.

CHAPTER 3

LITERATURE REVIEW

3.1 LITERATURE REVIEW

The electrolyte for solid oxide fuel cell must be stable in both reducing and oxidizing environments. It should have sufficiently high ionic with low electronic conductivity at cell operating temperature. The most advanced SOFCs are those based on the oxide ion conducting electrolytes. This chapter deals with the status of various oxide-ion electrolytes used in SOFCs and their advantages and disadvantages. The following research papers deals with recent work done in the field of solid electrolytes.

Chen *et al*. [18] has reported that yttria-stabilized zirconia (YSZ) electrolytes with diverse microstructures were prepared by using nano-size $(Y_2O_3)_{0.08}(ZrO_2)_{0.92}$ powders as precursors through conventional sintering in air. The electrolytes were tested by ac impedance spectroscopy to elucidate the contribution of intragranular and intergranular conductivity to calculate the total ionic conductivity of the sample. The intragranular conductivity and intergranular conductivity were correlated with the microstructures of the electrolyte to interpret the transportation of oxygen ions through the electrolyte. The intragranular conductivity was found to be dominated mainly by the relative density while the intergranular conductivity strongly depends on the grain size and grain boundary area of the electrolyte.

According to Brahim *et al.*[19] one of the present challenges for the commercialization of planar solid oxide fuel cell is the reduction of its operating temperature, which requires the optimization of the electrolyte nature viz stability and compatibility with the other parts of SOFC and ionic conductivity. Thin layer technology seems to be suitable to decrease the electrolyte resistance at lower operating temperatures but shortcomings. Bilayered electrolytes are proposed and studied in terms of electrical performance. They are constituted of a gadolinia-doped ceria (GDC) layer (the most suitable candidates for intermediate temperature (IT) solid oxide fuel cells (SOFC) in terms of ionic conductivity) protected by an ultra-thin YSZ layer (as electronic barrier).

Zhu and Fan [20] have synthesized 8 mol% yttria doped zirconia (8YSZ) nanocrystals at 200 °C, through a hydrothermal process for 24 h. Characterizations revealed that the as-synthesized 8YSZ powder was weakly agglomerated and had a surface area of 121 m^2/g with an average grain size of 9 nm. Sintering behaviors of the 8YSZ powder were studied via isothermal and non-isothermal experiments. It demonstrated that the powder has high sintering ability. The superior sinterability at lower temperature achieved in their study was mainly attributed to the high green density and homogeneity of the green bodies with narrow-distributed interparticle pore structure. The low sintering temperature is of great practical importance for improving film quality and facilitating co-sintering of 8YSZ films together with other SOFC components.

Stability of electrolyte is very crucial for the performance of SOFC. One possible method of improving the stability of YSZ is by increasing the yttria concentration [21]. They concluded that 8.5 mol% YSZ have comparable mechanical strength and ionic conductivity to conventional 8 mol% YSZ, but it shows improved stability. Moreover, the conductivity of samples with yttria contents of 8.5 mol% could not be changed but in case of lower doping of yttria in ZrO_2 leads diversing trend in conductivity. These results strongly suggest that optimal properties can be obtained with processing conditions.

The sintered samples doped with 8.0 mol% Y_2O_3 (8.0YSZ), 8.5 mol% Y_2O_3 (8.5YSZ), 9.0 mol% Y_2O_3 (9.0YSZ), 9.5 mol% Y_2O_3 (9.5YSZ) and 10.0 mol% Y_2O_3 (10.0YSZ) was synthesized by Hattori *et al*. [22]. Out of them 9.5- and 10.0YSZ showed no conductivity decrease even for the annealing period of 1000 h, while 8.0- and 8.5YSZ showed significant decrease with time although the initial conductivities were higher than those of 9.5- and 10.0YSZ. The 9.0YSZ showed only slight change in conductivity. The measurement of Raman spectra demonstrated that the deterioration in conductivity related to the gradual formation of fine tetragonal phase in the cubic phase. Consequently, 9.5YSZ was seemed to be optimum composition to use as the electrolyte material for solid oxide fuel cells application.

Anderson *et al*. [23] have studied the reactivity of yttria-stabilized zirconia (YSZ) with other component of SOFC such as $Ln_{0.8}Sr_{0.2}FeO_3$ (Ln= Sm, Pr, Nd and a mixed lanthanide

precursor) and $La_{0.8}M_{0.2}FeO_3$ (M=Ba, Sr, Ca). Except Ca all variants showed increased reactivity with YSZ. The reactivity either results in secondary phase formation or incorporation of Zr onto the perovskite B-site.

Ridder *et al*. [24] have revealed that the outermost surface layer of the yttria stabilised zirconia (YSZ) electrolyte in the solid oxide fuel cell plays an important role in the performance of the cell. By combining $^{16}O/^{18}O$ exchange experiments with quantitative surface analysis by low energy ion scattering spectroscopy (LEIS), the relation between the composition of the outermost atomic layer and the oxygen kinetics at the surface of the electrolyte can be studied. The results suggest a linear relation between an increasing amount of impurity oxides present at the surface and a decreasing oxygen exchange. Ceramics invariably contain glassy impurities, which segregate to the grain boundaries during sintering. Their results, however, showed that the accumulation is restricted to the outermost atomic layer and proceeds until complete coverage is obtained. This observation underlines the importance of the used surface analysis technique. The strong accumulation of the impurities at the surface is observed even in the purest YSZ materials available in market. A decrease of the total bulk impurity concentration by a factor of 10–100 is necessary to ensure that the YSZ surface cannot be covered completely by impurities. The amount of exchanged oxygen at the outermost surface layer reduces from 50% at a clean yttria stabilised zirconia surface to zero at a surface completely covered by impurity oxides. Although the oxygen exchange experiments pertain to a temperature of 500 °C it is believed that the impurity oxides also have a strong influence at higher temperatures on the performance of electrolytes.

CeO_2-based electrolytes are promising candidates for intermediate temperature range (~800^{o}C). However, they are prone to electronic conduction at low partial pressures of oxygen [25]. They described the effect of yttria stabilized zirconia (YSZ) additions on $(CeO_2)_{0.8}(GdO_{1.5})_{0.2}$ materials between 0 and 20 mol% YSZ [8 mol% YSZ (8YSZ) and 3 mol% YSZ (3YSZ)], on the ionic conductivity. For all examined samples, a single cubic-phase was observed. This phase is stable between room temperature and 800 °C. Addition of 1 and 5 mol% of 8YSZ and 3YSZ in CeO_2-based electrolytes shows ionic conductivity very

similar to pure ceria based system. However, the ionic domain increased from $P_{o2} = 10^{-15}$ to 10^{-17} atm, showing greater stability of the system containing YSZ.

Jiang *et al.* [26] have developed a Bi_2O_3 electrolyte doped with Dy_2O_3 and WO_3 (DyWSB) that exhibits a higher conductivity than that of 20 mol% ebria stabilized bismuth oxide (20ESB). The dopants were selected based on their polarizability and its effect on structural stability and conductivity.

Some new fast oxide ion conductors for low temperature applications (400–600°C) have been proposed Boivin [27] during recent years. These materials exhibit different structural features than the well-known zirconia-based electrolytes**.** For the development of efficient low temperature devices it is important to have a very active electrode system which must be able to support oxygen molecule dissociation and recombination at high current densities. The BIMEVOX materials offer the unique opportunity of being able to act both as the electrolyte and the electrodes, overcoming many chemical and mechanical problems which are being faced to the commercialize the SOFCs.

Boivin *et al*. [28] revealed that electrochemical separation of oxygen from air is a promising application as solid electrolytes. However, several important specifications are required in order to obtain an efficient separation device. First of all, the electrolyte material must exhibit a high conductivity at moderate temperature. From this point of view, a new family of materials called BIMEVOX ideally fulfils this condition. Secondly, a typical separation device must comport two electrodes on opposite faces of the electrolyte**.** These electrodes must act as electronic collectors but also, at the cathodic side, as an oxygen dissociation catalyst. BIMEVOX electrolytes exhibit high ionic conductivity which can be allowed to work at low temperature (~500°C). The classical electrode approach, like in solid oxide fuel cells, consists a specific mixed oxide, for instance, strontium lanthanum magnetite or cobaltite. However, the lower the temperature, the lower the efficiency of these electrodes which quickly appears as the limiting factor. In previous work on bismuth lead oxide electrolytes, he proposed a new approach that consists of using the surface of the bismuth-based electrolyte itself as the catalyst, the electron collection being then performed by a co-sintered metallic grid. This ‘in-situ' electrode system provides many advantages, particularly

it eliminates the problem of the chemical compatibility between electrode and electrolyte materials.

Dygas *et al.* [29] studied the impedance of a polycrystalline sample of $Bi_2V_{0.9}Cu_{0.1}O_{5.35}$, sintered from crushed single crystals, was measured in air in the frequency range 3.2 mHz to 10 MHz at constant temperatures up to 707°C using an automated setup which allowed measurement of high impedances. The measured spectra were simulated by least-squares fitting of equivalent circuits. A time dependence of conductivity was found in a limited temperature range similar to the earlier observations for single crystals. Prolonged annealing at about 427°C resulted in a low conductivity state at low temperatures, while the high conductivity state was recovered upon heating to 557°C. The values of conductivity were only independent of the thermal history of the polycrystalline sample above 557°C. Conductivity of polycrystalline materials is lower by about a factor 2, than the conductivity of the single crystal measured in the direction parallel to the layers of the intergrowth structure. Separation of the total resistance into intragrain and intergrain components was feasible only in the high conductivity state of the polycrystalline sample at temperatures below 397°C.

According to Simner *et al.* [30] copper-substituted bismuth vanadate ($Bi_2V_{0.9}Cu_{0.1}O_{5.35}$), known as BICUVOX, possesses high oxygen ion conductivities at low temperatures. The ionic conductivity of this material at 300^0C (~$1x10^{-3}$S/cm) is 50 to 100 times greater than any other solid electrolyte in this temperature range. A BICUVOX.10 composition was synthesized by conventional solid-state reaction methods. Sintering of the powders at 800^oC for 10 to 20 h produced ceramic monoliths possessing greater than 95% of theoretical density. The densified ceramics displayed an equiaxed microstructure of less than 10μm grain size with no evidence of exaggerated grain growth despite the lengthy sintering time. The materials prepared in these studies exhibited the high ionic conductivity which is the characteristic of the Cu-doped $Bi_4V_2O_{11}$ system .The non-Arrhenius behavior of the conductivity was correlated with DTA measurements which indicated that reversible transformations occurred in the same temperature change as the change in slope of the conductivity- temperature curve. Isothermal heating of samples at 450^oC and 500^oC indicated no significant change in conductivity over prolonged periods of time. The magnitude of the

conductivity, its ability to prepare high- density ceramics make the BICUVOX material a very promising solid electrolyte system for lowering the operating temperatures of electrochemical oxygen generators with other electrochemical applications.

Quoc Pho and Thah Son [31] have obtained the electrical conductivity of fast ion conducting system BIMEVOX ($Bi_2Me_x\ V_{1-x}O_{5-1.5x}$) as a function of temperature using ac impedance spectroscopy. The ionic conductivity of single crystal was investigated and compared with values from ceramic pellets. It had been shown that large electrical anisotropy between the directions parallel and perpendicular to the $(Bi_2O_2)^{2+}$ layer of BIMEVOX single crystal were obtained. The anisotropy coefficient depends on the composition. For the compound of nominal composition $Bi_2V_{0.9}Cu_{0.1}O_{5.35}$ at 500^{o}C, the conductivity along the direction parallel to the $(Bi_2O_2)^{2+}$ layer is two orders of magnitude larger than along the direction perpendicular to the $(Bi_2O_2)^{2+}$ layer.

Vannier *et al.*[32] have prepared and characterized three types of solid solutions derived from $Bi_4V_2O_{11}$: $Bi_2V_{1-x}Pb_xO_{(11-3x)/2}$ with x up to 0.01, $Bi_2PbyVO_{(11-y)/2}$ with y up to 0.20 and $Bi_2Pb_{.1+x}V_{1-x}O_{(10.9-3x)/2}$ with x up to 0.12. A single crystal X-ray structure determination was performed on a sample corresponding to the formula $Bi_{1.9}Pb_{0.2}V_{0.9}O_{5.3}$. The material was shown to be isostructural with BICUVOX.10 (γ-$Bi_4V_2O_{11}$). The ability of substitution of V by Pb was confirmed. Conductivity measurements led to the values of conductivity (σ) close to that of BICUVOX.10 at high temperature, but significantly lower performances at low temperature. This was related to a decrease of the stability of the γ form in the lead substituted phases.

Pernot *et al*. [33] studied that the partially Cu- or Ni-substituted compounds ($Bi_4V_{2(1-x)}M_{2x}O_{(11-3x)}$; M=Cu, Ni) are highly oxygen conducting. Three phases are observed in the unsubstituted compound i.e. α, β and γ phases at room temperature 400 and 550^{o}C respectively. Structure and conductivity are studied as a function of substitution on the vanadium sites between 0 and 6 mol% at room temperature, the Cu compound remains in the orthorhombic α phase and its ionic conductivity increases. A strong anisotropic conductivity behaviour is also observed in these samples.

Joubert *et al*. [34] have investigated two new BIMEVOX series $Bi_4V_{2-x}M_xO_{11-x}$ (M= Cr^{III}, Fe^{III}) by X-ray powder diffraction, thermal analysis and ionic conductivity measurements. Structural phase transitions α↔β and β↔γ occurs as a function of composition and temperature in iron substituted phases for which a new orthorhombic domain is evidenced when x exceeds 0.5. At low temperature, the Cr compounds retain the α orthorhombic symmetry

According to Yaremchenko *et al*.[35], the fluorite-type oxygen-ion conducting solid solutions $(Bi_{1-x}Zr_x)_{0.85}Y_{0.15}O_{1.5+\delta}$ (x = 0.05 and 0.07) and $(Bi_{0.95}Nb_{0.05})_{0.85}Ho_{0.15}O_{1.5+\delta}$ are partially decomposed below 627^oC temperatures, forming several phases such as to δ- and γ-Bi_2O_3. Formation of the bcc γ- Bi_2O_3- -type phases at 497^oC leads to a sharp decrease in conductivity. Interaction of the Bi_2O_3-based solid electrolytes with silver electrodes was observed at temperatures above 577^oC, resulting in increasing resistance of the electrochemical cells. Electrodes of platinum and perovskite-type $La_{0.7}Sr_{0.3}CoO_{3-\delta}$ were ascertained to exhibit sufficient stability when in contact with the bismuth oxide-based electrolytes in the temperature range of 597–727 ^oC.

Abrahams *et al*. [36] discussed the defect structure of the BIMEVOXes and construct general defect equqtions for formation of solid solution. Two limiting models were proposed by which solid solution formation can occur. In the equatorial vacancy (EV) model, vacancies are located exclusively in the bridging sites in the vanadate layer. In contrast, the apical vaccancy (AV) model assumes vacancies are located exclusively in non-bridging apical sites in the vanadate layer. The general defect equations can be used to predict theoretical solid solution limits for all types of substitutions for vanadium in $Bi_4V_2O_{11-\delta}$. These limits are found to vary not only with charge of the dopant ion, but also with the coordination number of the metal dopant. In most cases it is found that the EV model yields theoretical solid solution limits close to those observed. The EV model is also used to present a mechanism for ionic conduction in BIMEVOX, which involves movement of equatorial oxide ions/vacancies between vanadium octahedral and tetrahedra with the formation of five coordinate vanadium intermediate systems.

Yan *et al.* [37] prepared $Bi_4V_{2-x}M_xO_{11-x/2}$ (M= Ti, Zr, Sn, Pb) by solid state reactions. They observed that all the substituted phases retain the α-phase for $x < 0.20$. When $x \geq 0.20$, the high oxygen ionic conducting γ-phase is stabilized at room temperature. The higher conductivity of the substituted phases compared with the parent compound of $Bi_4V_2O_{11}$. High conductivity of substituted system may be correlated with increased oxygen vacancies generated by aliovalent substitutions. The highest ionic is observed conductivity in Ti substituted system. It can be attributed to its lower activation energy.

Vannier *et al.* [38] studied $Bi_4V_2O_{11}$ powdered samples and single crystals. These systems were characterized by high temperature X-ray diffraction and impedance spectroscopy. From high temperature X-ray diffraction on powders and single crystals, the α↔β and β↔γ reversible phase transitions were observed..

Lee *et al*. [39] has reported that the phase $Bi_4V_2O_{11}$ is a solid solution whose composition covers the range ~ 66.7 to 70.4% Bi_2O_3. The high temperature γ polymorph is an excellent oxide ion conductor, whose conductivity decreases gradually with increasing Bi_2O_3 content. The low temperature α polymorph is a ferroelectric whose permittivity appears to increase to a maximum at α↔β transition temperature.

The compositional ranges of $Bi_4V_2O_{11}$ solid solutions containing rare earth elements (Nd, Gd, Er and Yb) were determined by means of a phase diagram [40]. The locus of the solid solutions indicates that rare earth elements replace V in the crystal structure and the new family of oxide ion conductors has the overall formula $Bi_{4+y}V_{2-x-y}M_xO_{11-y-x}$. DTA studies confirmed the identity of the various polymorphs formed in this system. AC impedance studies show that Nd-, Gd-, Er- and Yb-doped materials are oxide ion conductors; however, they are electrically inhomogeneous. The best conductors, irrespective of the dopants, have compositions with y = 0 and x = *0*.2 with conductivity values of up to $2 \times 10^{-4}\Omega^{-1}cm^{-1}$ at 300^oC.

From the literature review discussed above, it is seen that YSZ is the most commonly used electrolyte in solid oxide fuel cells and one of the challenges for the commercialization of planar solid oxide fuel cell is the reduction of its operating temperature, which requires the

optimization of the electrolyte which has good stability and higher ionic conductivity in intermediate temperature range. Some of the papers reveal that YSZ electrolyte shows optimum conductivity at higher temperatures (~1000^{o}C) which causes the aging effects in electrolytes and also degradation of electrolytes. CeO_2-based electrolytes are promising candidates for intermediate temperature range. However, they are prone to electronic conduction at low partial pressures of oxygen. According to rest of papers a new family of materials called BIMEVOX exhibit a high conductivity at moderate temperature with good stability.

The aim of the present work is to synthesize and characterize an electrolyte which exhibit higher ionic conductivities at low temperatures and shows less aging effects. In present studies, a series of $Bi_{4-x}M_xV_2O_{11}$ ($0 \leq x \leq 0.4$) samples was synthesized by solid state reaction method. These samples were characterized by various techniques to study the effect of dopant and its concentration on structural, thermal and electrical properties of Bismuth Vanadate.

CHAPTER 4

EXPERIMENTAL TECHNIQUES

General

The brief details on sample preparation and characterization techniques are presented in this chapter that was adopted during the course of the present investigations.

4.1 Sample preparation

The Bi_{4-x} $La_xV_2O_{11}$ and Bi_{4-x} $Gd_xV_2O_{11}$($0 \leq x \leq 0.4$) powders were prepared by solid state reaction from stoichiometric amounts of the Bi_2O_3, V_2O_5, La_2O_3, Gd_2O_3 oxides. The purity of all the oxides was more than 99%. The mixture of starting powders was ball-milled by using apparatus shown in Fig 4.1, using porcelain milling media for 2 hrs in acetone media after manually mixing in mortar pestle for half an hour. This length of time was required to achieve a fully homogeneous powder mixture and to facilitate good reaction of the oxide powders. The resulting mixture was dried, thoroughly ground to break up any large agglomerates, and then heat treated at 700^oC in silica crucible for 12 hrs. To ensure complete reaction the materials again ground and heat treated at 800^oC in a silica crucible for 12 hrs. Green preforms were formed by uniaxially cold pressing 6g powder of Bi_{4-x} $M_xV_2O_{11}$ (M= La, Gd) to a load of 10 ton. The approximate pellets dimensions were 20 mm diameter by 3 mm thickness. The disc shaped pellets were sintered at 800^oC for 10 hrs and then allowed to cool in furnace.

Figure 4.1: *Apparatus used for Ball-Milling*

Flowchart for sample preparation

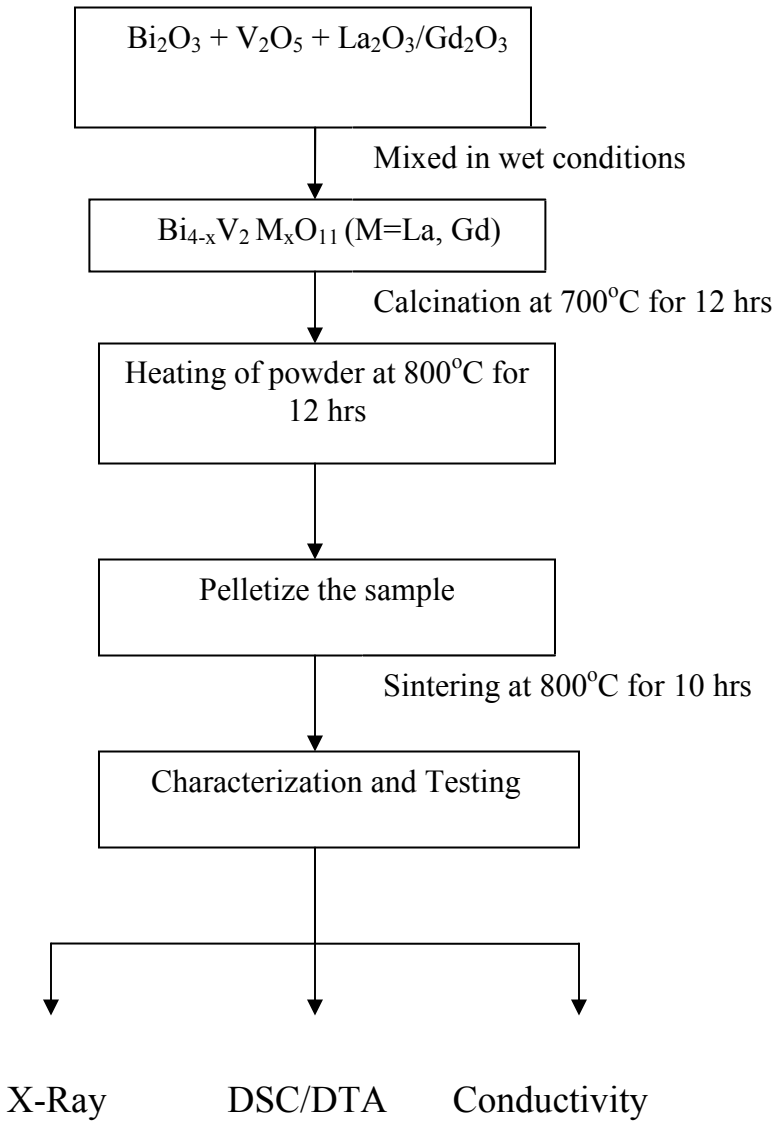

4.2 Characterization

The samples were characterized using X-ray diffraction (XRD), differential scanning calorimetry (DSC), thermo gravimetric analysis (TGA) and ac-impedance spectroscopy. The details of characterization techniques are given below:

4.2.1 Structural characterization

Structural investigations of the samples were carried out through X-ray diffraction. The X-Ray diffraction patterns were recorded using Rigaku model Geiger diffractogram with CuK_{α} radiation ($\lambda = 1.5418A^{o}$) obtained from a copper target using an inbuilt Ni monochromatic filter. The XRD patterns were generally taken in the range of $5^{o} \leq 2\theta \geq 100^{o}$ for most of the samples at a scan rate of 5 degree per minute. The inter-planar spacing (d) values of samples were calculated using the Bragg's law:

$$2d \sin \theta = n \lambda \tag{10}$$

The XRD patterns of all the samples are identified using Powder diffraction files (PDF) for various crystalline phases. The lattice parameters of samples are calculated by using following equation

$$1/d^2 = h^2/a^2 + k^2/b^2 + l^2/c^2 \tag{11}$$

where h, k, l are miller indices and a, b, c are lattice parameter for orthorhombic system.

4.2.2 Thermal Analysis

Thermal analysis is a technique in which a physical property of a substance is measured as a function of temperature or time while the substance is subjected to a controlled- temperature programme. The two main thermal analysis techniques that are used in the present study are thermo gravimetric analysis (TGA) and the differential scanning calorimetry (DSC).

TGA gives information about the composition, moisture content, and degradation of materials at high temperatures. TGA is a technique by which the mass of a substance is measured as function of temperature or time while the substance is subjected to a controlled - temperature program in a specified environment. However, in case of DSC measurement

enthalpy is measured with respect to the temperature.

The TGA and DSC measurements were carried out on Thermal Analysis instrument model SDTQ600

4.2.3 Electrical Conductivity

Electrical conductivity was analyzed using complex impedance spectroscopy. An ac two – probe impedance measurement technique was employed using a Hewlett-Packard precision LCR meter Model HP 4247A in the frequency range of 100Hz to 100 kHz. For conductivity measurements, the disc shaped pellets were gold sputtered onto the surface of the disc in vacuum. Sample conductivity was measured with respect to temperature at 20^{o}C intervals on cooling from 700^{o} to 200^{o}C. The sample was kept in between the copper circular disc of sample holder as shown in figure 4.3.

Figure 4.2: *Setup for the conductivity measurement*

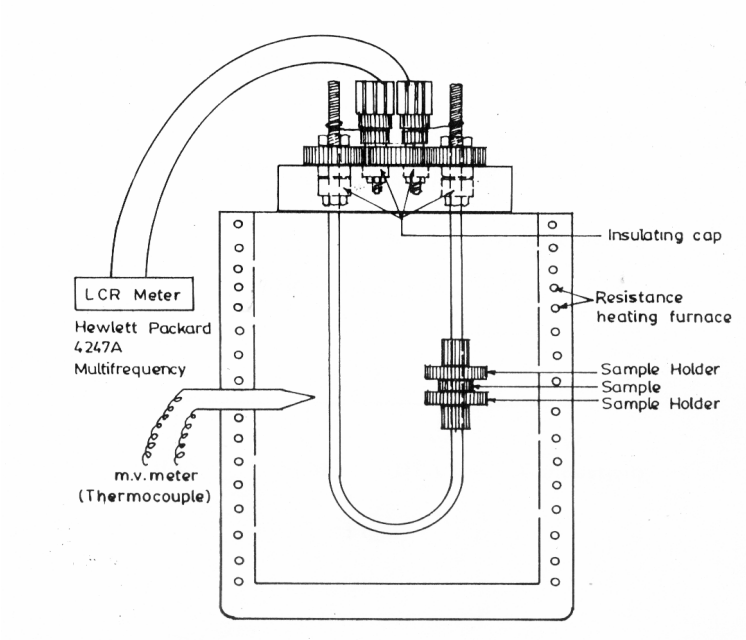

Figure 4.3: *Arrangement of Sample holder in the furnance*

Analysis of conductivity data is often carried out by complex plane methods which involve the plotting of imaginary part of Z″ against the real part Z′ when plotted on the linear scale. The plot usually forms a semicircle or spikes (cole - cole plot). From the interception of plot on the x-axis, the true bulk resistance can be calculated. Values of the bulk conductivity will be obtained from the estimated values of R_b.

CHAPTER 5

RESULTS AND DISCUSSION

5.1 X-ray Analysis

The X-ray diffraction (XRD) pattern of $Bi_4V_2O_{11}$ (Fig 5.1) shows the characteristic doublets at $2\theta \approx 31^o$, 39^o, 48^o, 54^o and a very weak reflection at $2\theta \approx 24.2^o$. This weak reflection is attributed to the superstructure of α-$Bi_4V_2O_{11}$ [36]. All the observed reflections excluding this weak reflection could be indexed on an orthorhombic unit cell, and this unit cell was considered as the mean or the basis cell of this α-$Bi_4V_2O_{11}$. The mean cell parameters for this phase are $a_m \approx 5.530\pm0.003$, $b_m \approx 5.606\pm0.002$ and $c_m \approx 15.282\pm0.007^oA$ (where m is the mean cell). Joubert *et al*. [34], has reported that the structure of $Bi_4V_2O_{11}$ is monoclinic which is closely related to the earlier reported orthorhombic lattice. The striking feature of the monoclinic pattern is the presence of a characteristic doublet between $2\theta \approx 45.5$ and 46.5^o which is a singlet in the orthorhombic pattern. In present samples, we could not observed doublet peaks in this range which indicates that the unit cell is orthorhombic. The X-ray powder diffraction data confirmed that samples of $Bi_{4-x}La_xV_2O_{11}$ and $Bi_{4-x}Gd_xV_2O_{11}$ prepared by solid state reaction method are single phase with orthorhombic unit cells for the composition ($0 \leq x \leq 0.4$). The XRD pattern of $Bi_{4-x}La_xV_2O_{11}$ and $Bi_{4-x}Gd_xV_2O_{11}$ for x=0, 0.1, 0.2 and 0.3 could be indexed with α-$Bi_4V_2O_{11}$ [34] with lattice parameters comparable to the reported ones. It is revealed that first three compositions, in both cases exhibited, α-phase except some peak broadening and peak shifting at lower 2θ values. It can be seen from the XRD patterns that with the increase in the impurity concentration the peak width and the peak intensity decreases as shown in Fig. 5.2 and 5.3. For the impurity concentration (x=0.4) the α- phase is converting into β- phase as there is a shifting of peak to the lower 2θ. It could be indexed as β-$Bi_4V_2O_{11}$ phase. β-$Bi_4V_2O_{11}$ phase is tetragonal cell with parameters a = b=

11.24±0.02 (^oA) and c = 15.45±0.02 (^oA) [44].

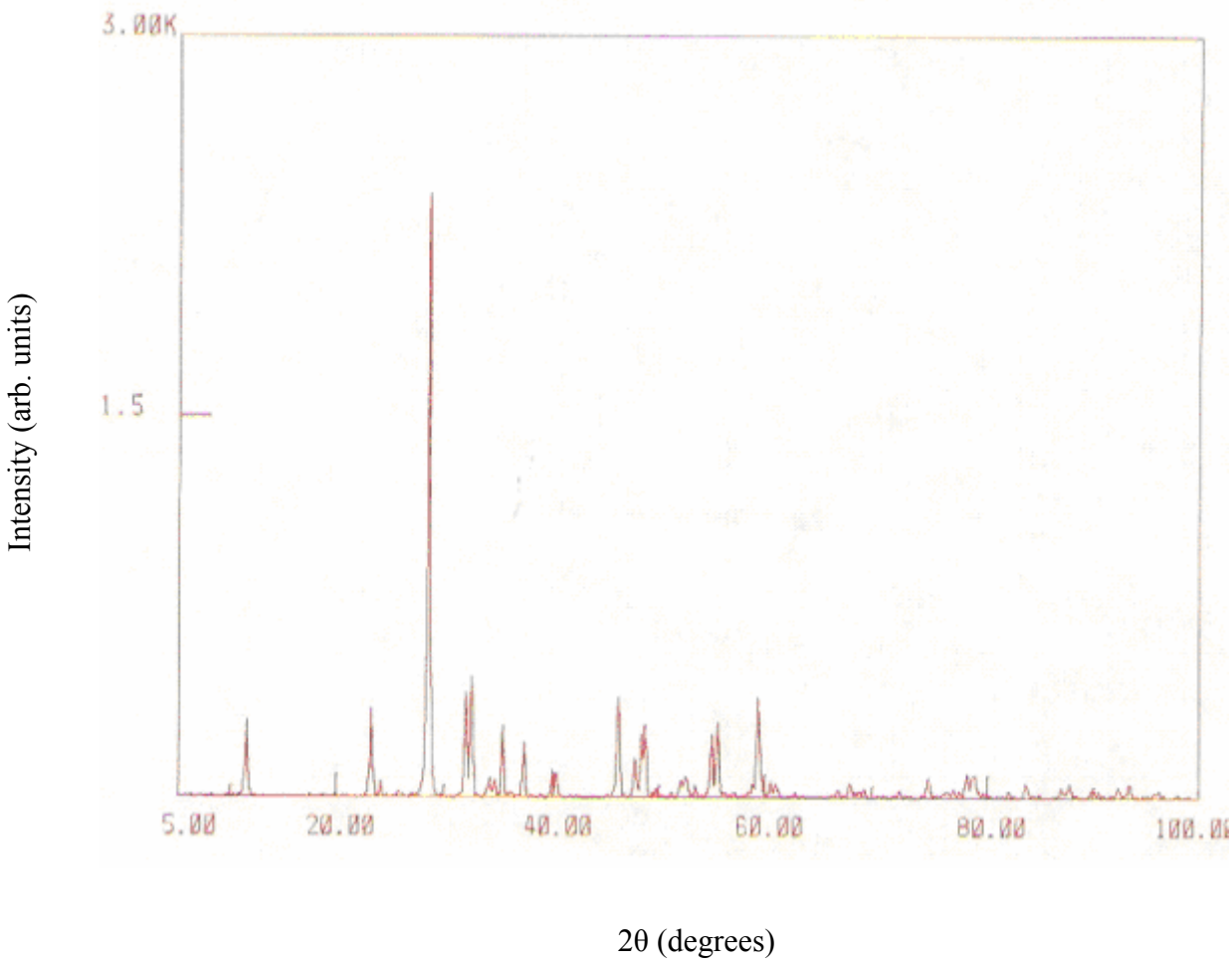

Figure 5.1: *X-ray diffraction pattern of pure* $Bi_4V_2O_{11}$

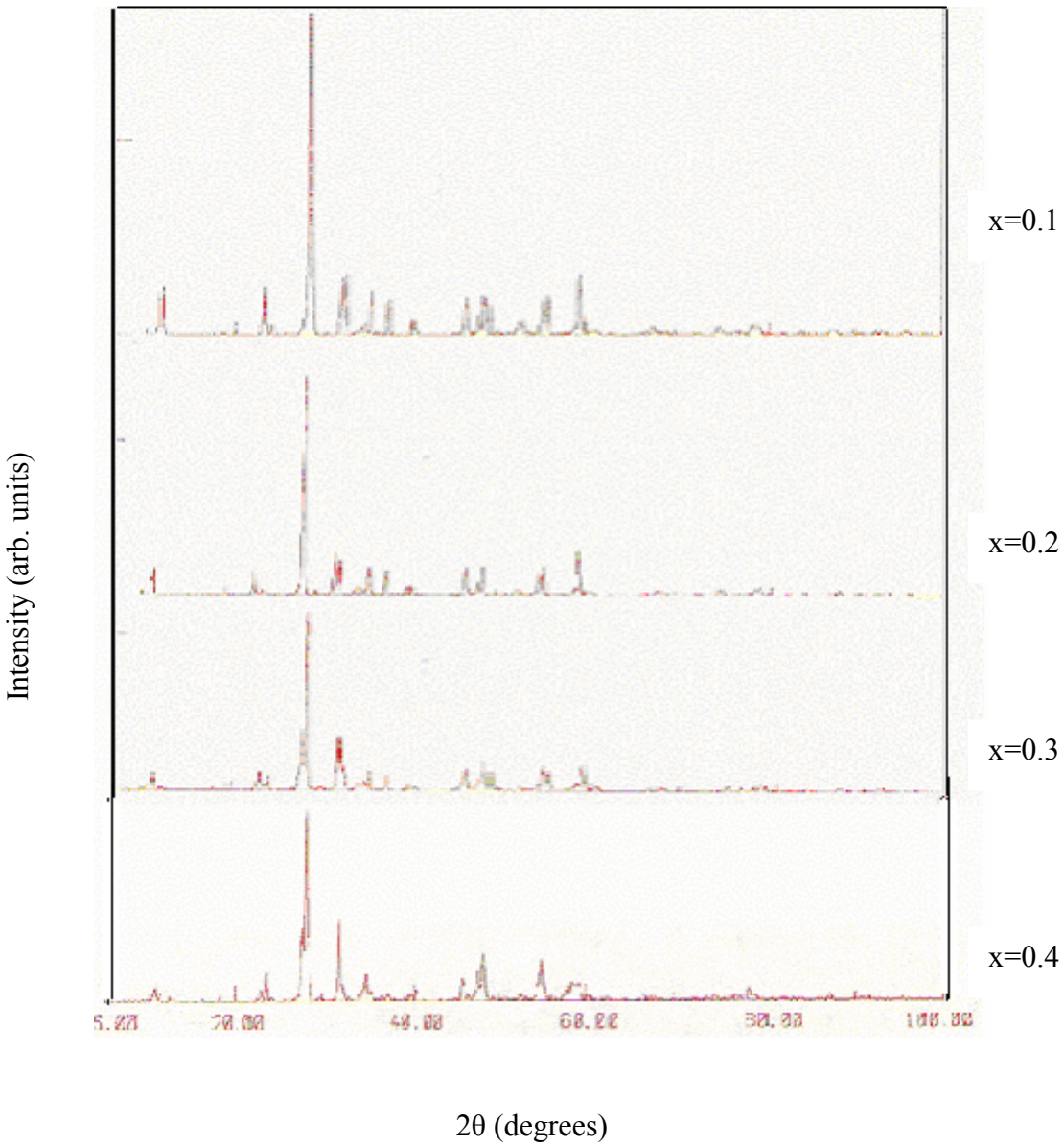

Figure 5.2: *X-ray diffraction pattern of $Bi_{4-x}La_xV_2O_{11}$ (for x= 0.1, 0.2, 0.3 and 0.4)*

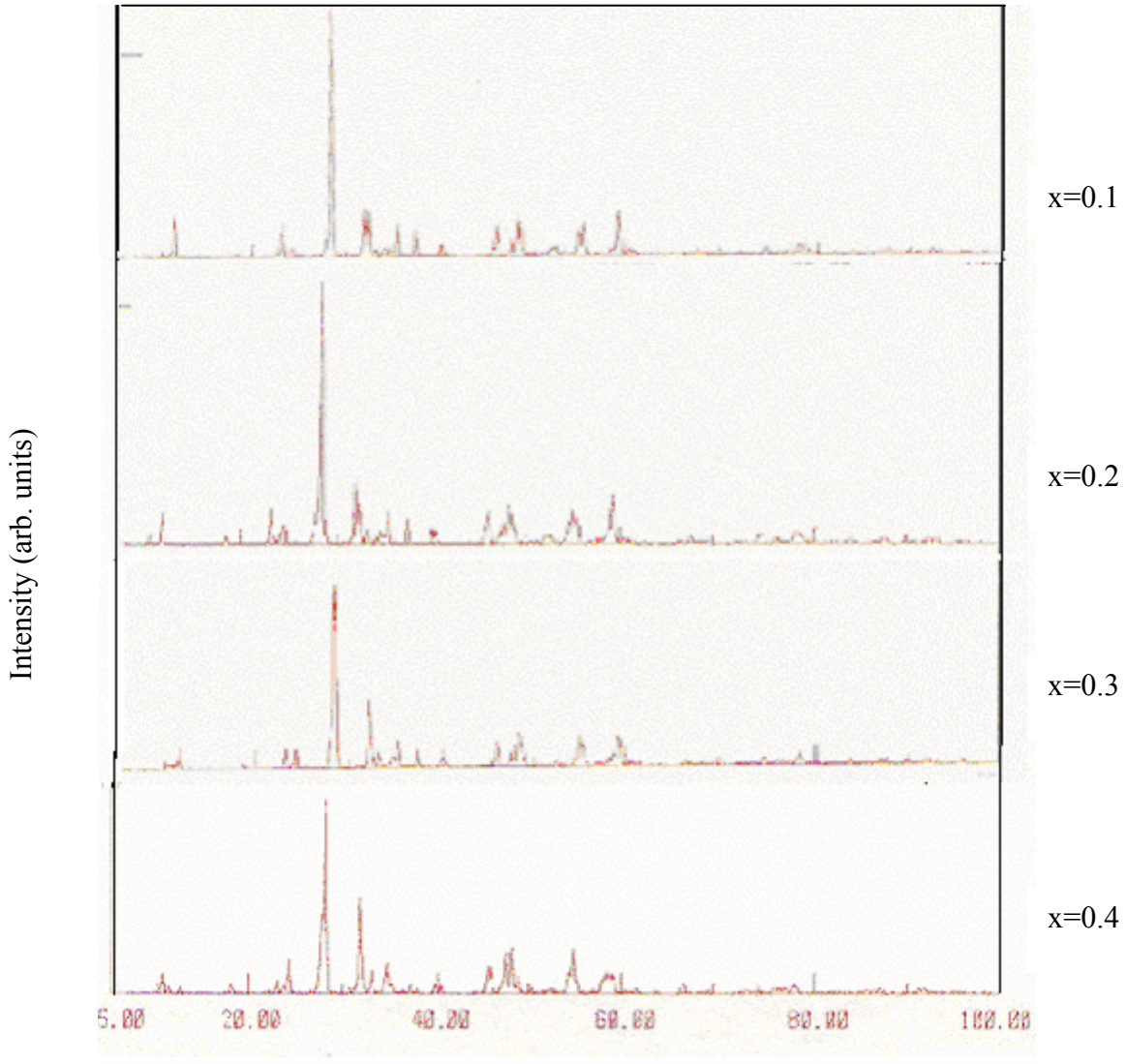

Figure 5.3: *X-ray diffraction pattern of* $Bi_{4-x}Gd_xV_2O_{11}$ *(for x= 0.1, 0.2, 0.3 and 0.4)*

The lattice parameters (in A^o) derived from X-Ray powder diffraction patters are given in the table below.

Table1 Lattice parameters for $Bi_{4-x}La_xV_2O_{11}$ ($0 \leq x \leq 0.4$)

Composition	a (A^o)	b(A^o)	c(A^o)
x=0	5.53	5.61	15.25
x=0.1	5.52	5.60	15.26
x=0.2	5.53	5.60	15.34
x=0.3	5.53	5.61	15.26
x=0.4	11.24	11.26	15.43

Table2 Lattice parameters for $Bi_{4-x}Gd_xV_2O_{11}$ ($0 \leq x \leq 0.4$)

Composition	a (A^o)	b(A^o)	c(A^o)
x=0	5.53	5.61	15.25
x=0.1	5.54	5.60	15.36
x=0.2	5.54	5.59	15.34
x=0.3	5.54	5.57	15.43
x=0.4	11.24	11.23	15.45

The variation of lattice parameters with the increase in impurity concentration for lanthanum and gadolinium system is shown in figure 5.4 to 5.7.

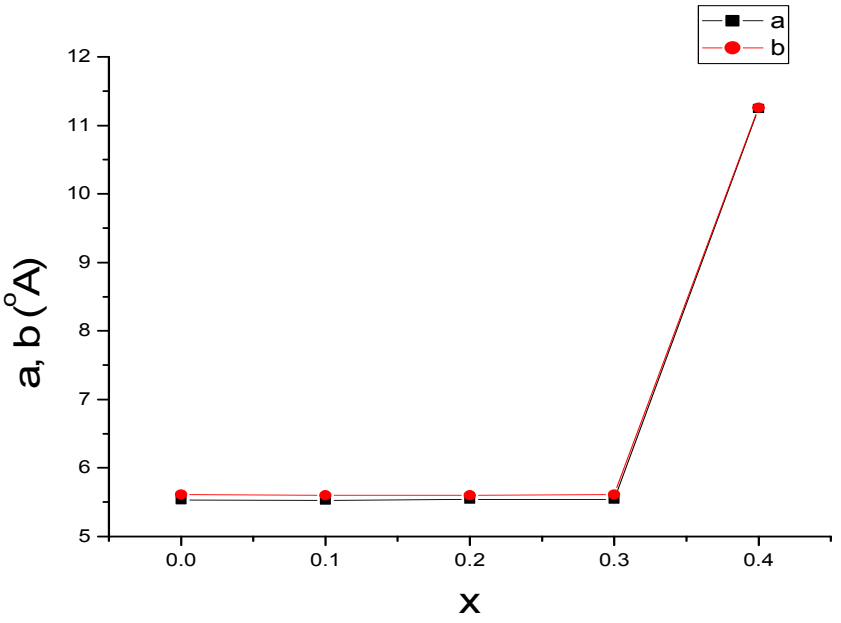

Figure 5.4: *Variation of lattice parameters a, b for $Bi_{4-x}La_xV_2O_{11}$ with doping concentration*

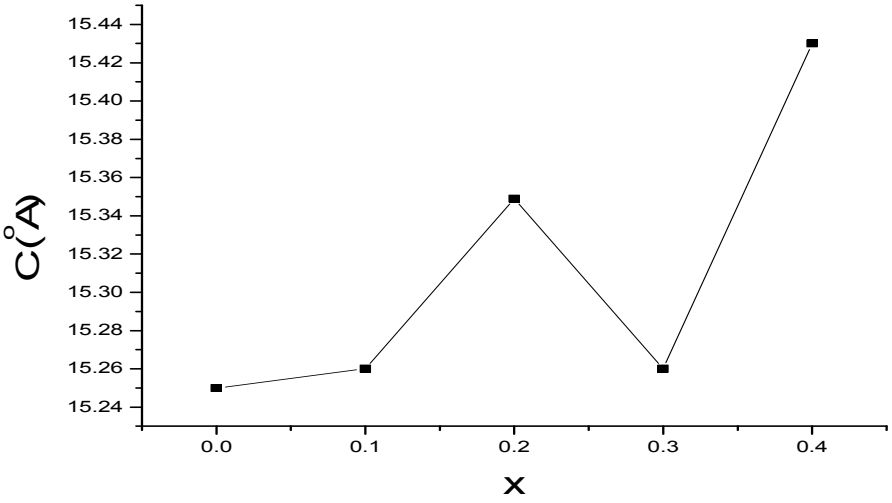

Figure 5.5: *Variation of lattice parameters c for $Bi_{4-x}La_xV_2O_{11}$ with doping concentration*

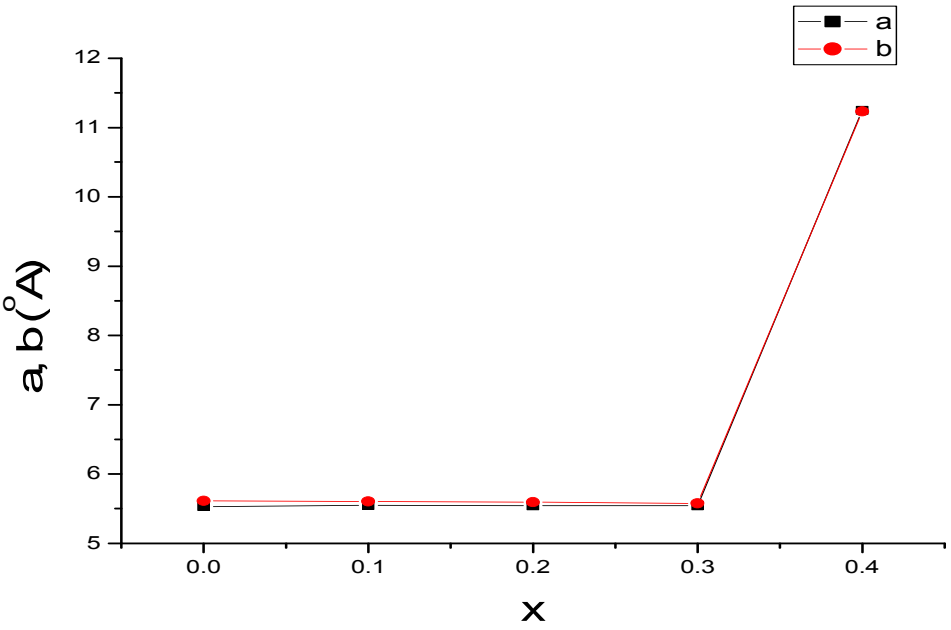

Figure 5.6: *Variation of lattice parameters a, b for $Bi_{4-x}Gd_xV_2O_{11}$ with doping concentration*

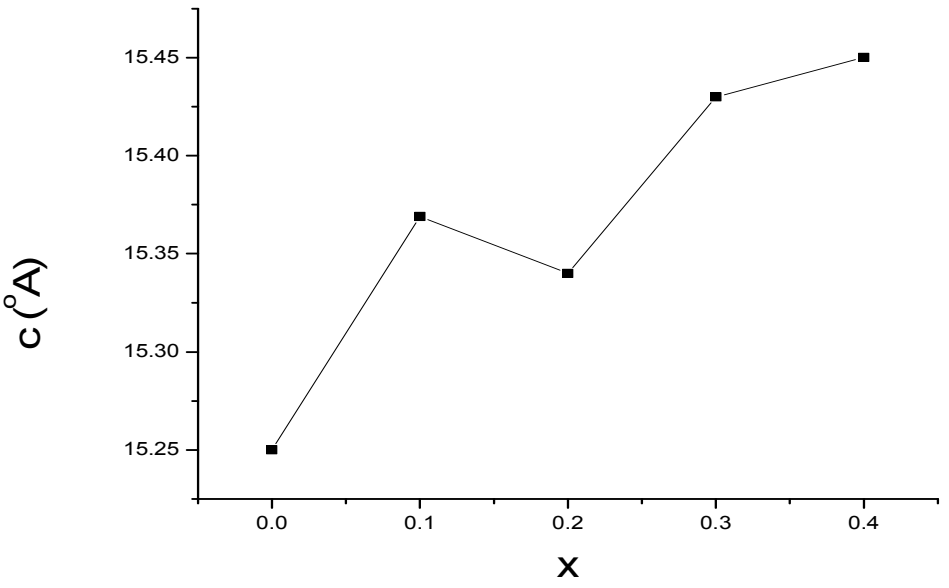

Figure 5.7: *Variation of lattice parameters c for $Bi_{4-x}Gd_xV_2O_{11}$ with doping concentration*

The lattice parameters of samples $Bi_{4-x}M_xV_2O_{11}$ ($0 \leq x \leq 0.3$), with both the substitution, could not show any significant change as indicated in table 1 and 2 as well as in Fig. 5.4 to 5.7. It is shown from Fig. 5.4 and 5.6 that there is a rapid change in lattice parameters of x=0.4 sample as compared to $Bi_{4-x}M_xV_2O_{11}$ ($0 \leq x \leq 0.3$) samples, similar results has been observed by Joubert *et al* [34]. The change in a, b lattice parameter of x=0.4 sample is due to phase transformation from α-$Bi_4V_2O_{11}$ to the β-$Bi_4V_2O_{11}$.

5.2 Thermal Analysis

The present samples were also tested by thermogravimetric and differential calorimetry analysis (DSC). TGA and DSC curve indicated striking similarity in their behaviour in all the samples. However, phase transformation peaks are very clear in DSC curves as compared to TGA curves. Figures 5.8 to 5.16 show DSC and TGA curve of $Bi_{4-x}M_xV_2O_{11}$ (M= Gd, La) sample. DSC curve of pure sample (x= 0.0) exhibit two endothermic peaks at 440^oC and 552^oC, which clearly indicates the transformation of α→β and β→γ phase [42]. However, the second endothermic peak is very weak than peak observed at 440^oC. The DSC curves for x= 0.1, 0.2 and 0.3 show a small but noticeable peak at about 400^oC. This may be attributed to the α→β transitions in these samples. In contrast to x = 0.0 sample the phase transition from β→γ does not exist in these samples except $Bi_{3.7}La_{0.3}V_2O_{11}$ sample. In particular sample, an endothermic peak also exhibit at ~ 580^oC. It may be due to the β→γ phase transformation with shifting at higher side of the temperatureas reported by other researchers for β→γ phase transition [42]. In case of x = 0.4 sample a broad endothermic peak has been observed at 500^oC in both the samples i.e. $Bi_{3.6}La_{0.4}V_2O_{11}$ and $Bi_{3.6}Gd_{0.4}V_2O_{11}$. Intrestingly, the DSC peak is shifted at higher temperature and observed at ~ 500^oC which may be attributed to β→γ phase transition in this sample.

This is consistent with the X-ray diffraction pattern of these samples [33] which indicated the β-phase stabilization at room temperature.

DSC-TGA

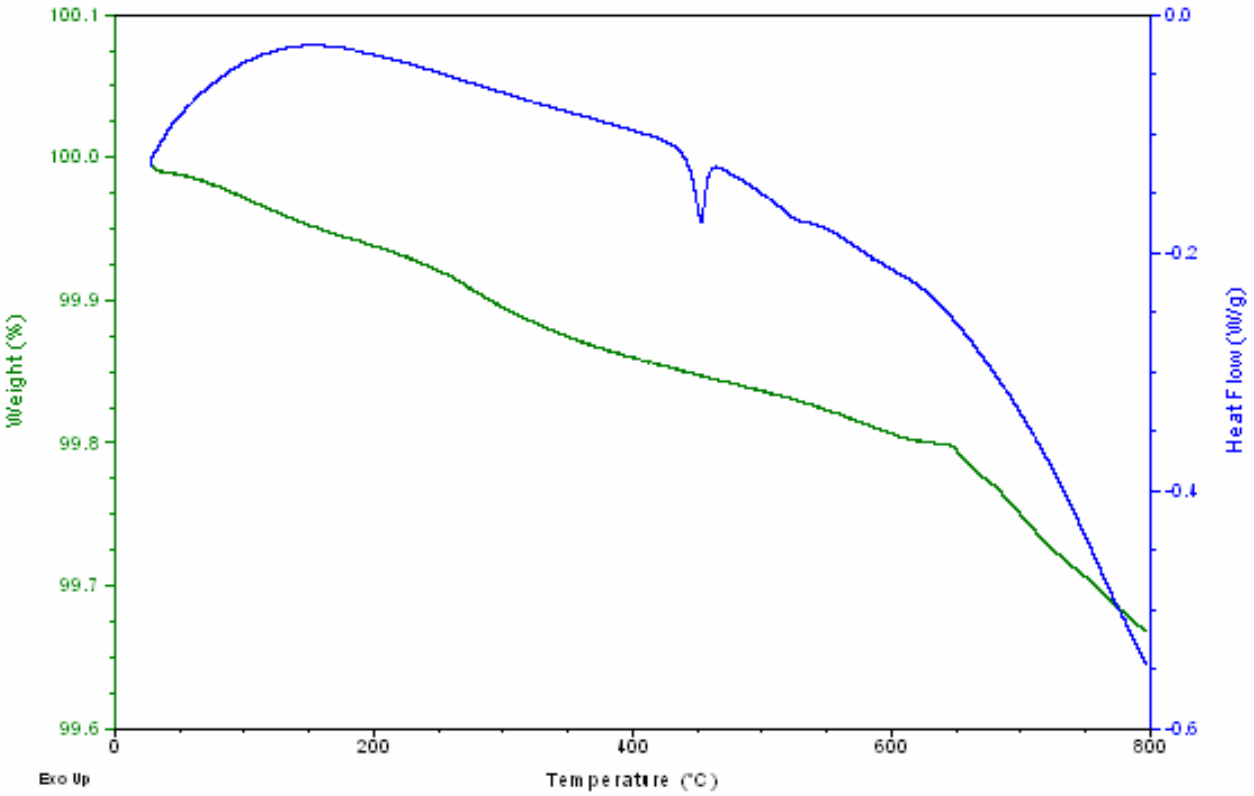

Figure 5.8: *DSC thermograph for sample* $Bi_4V_2O_{11}$

DSC-TGA

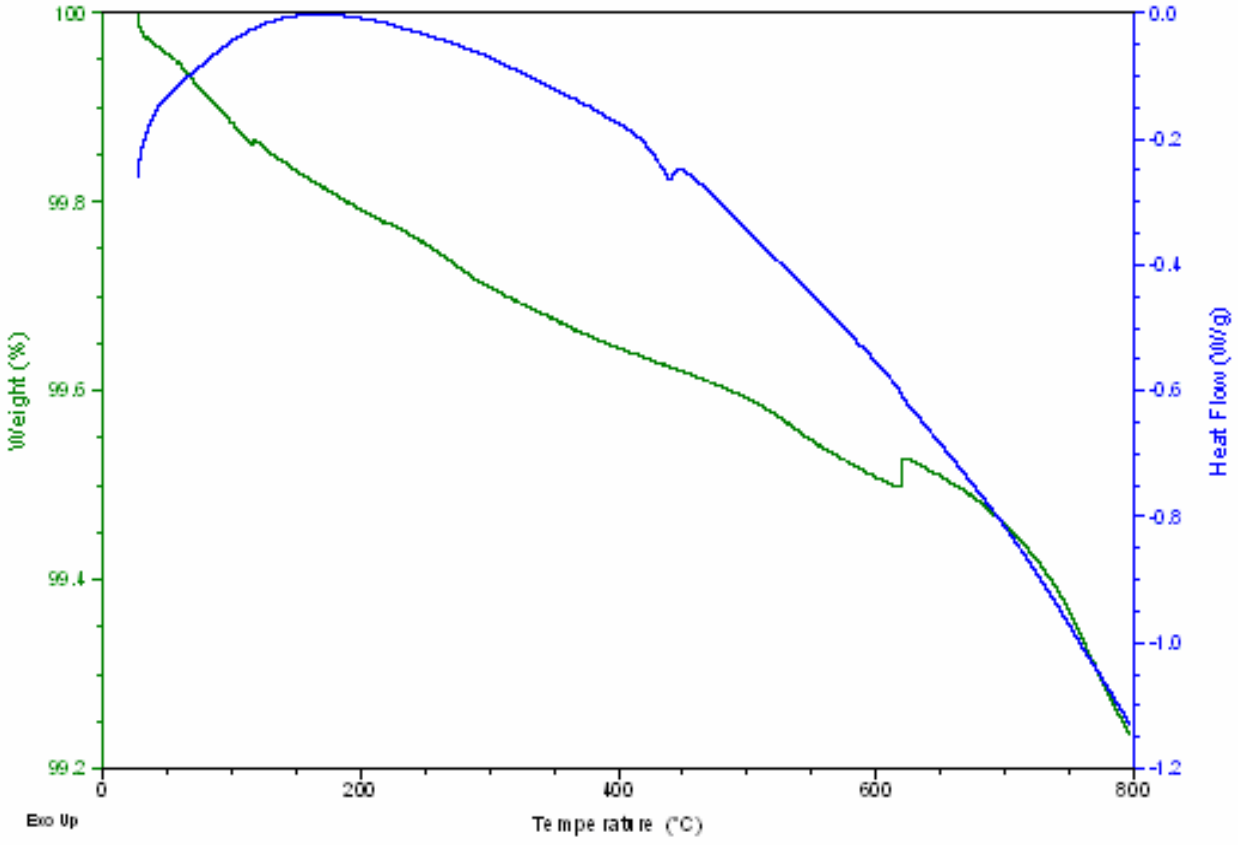

Figure 5.9: *DSC thermograph for sample* $Bi_{3.9}La_{0.1}V_2O_{11}$

DSC-TGA

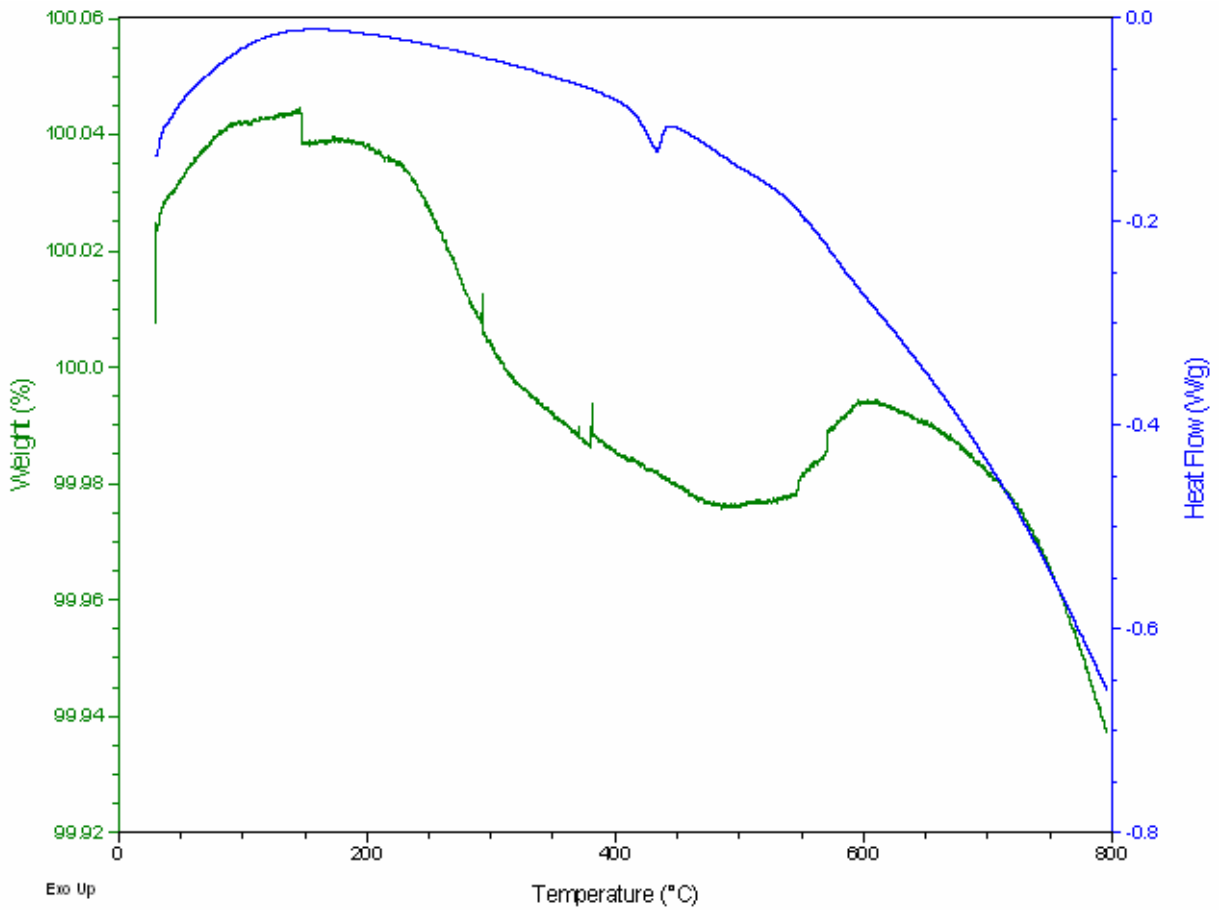

Figure 5.10: *DSC thermograph for sample* $Bi_{3.8}La_{0.2}V_2O_{11}$

DSC-TGA

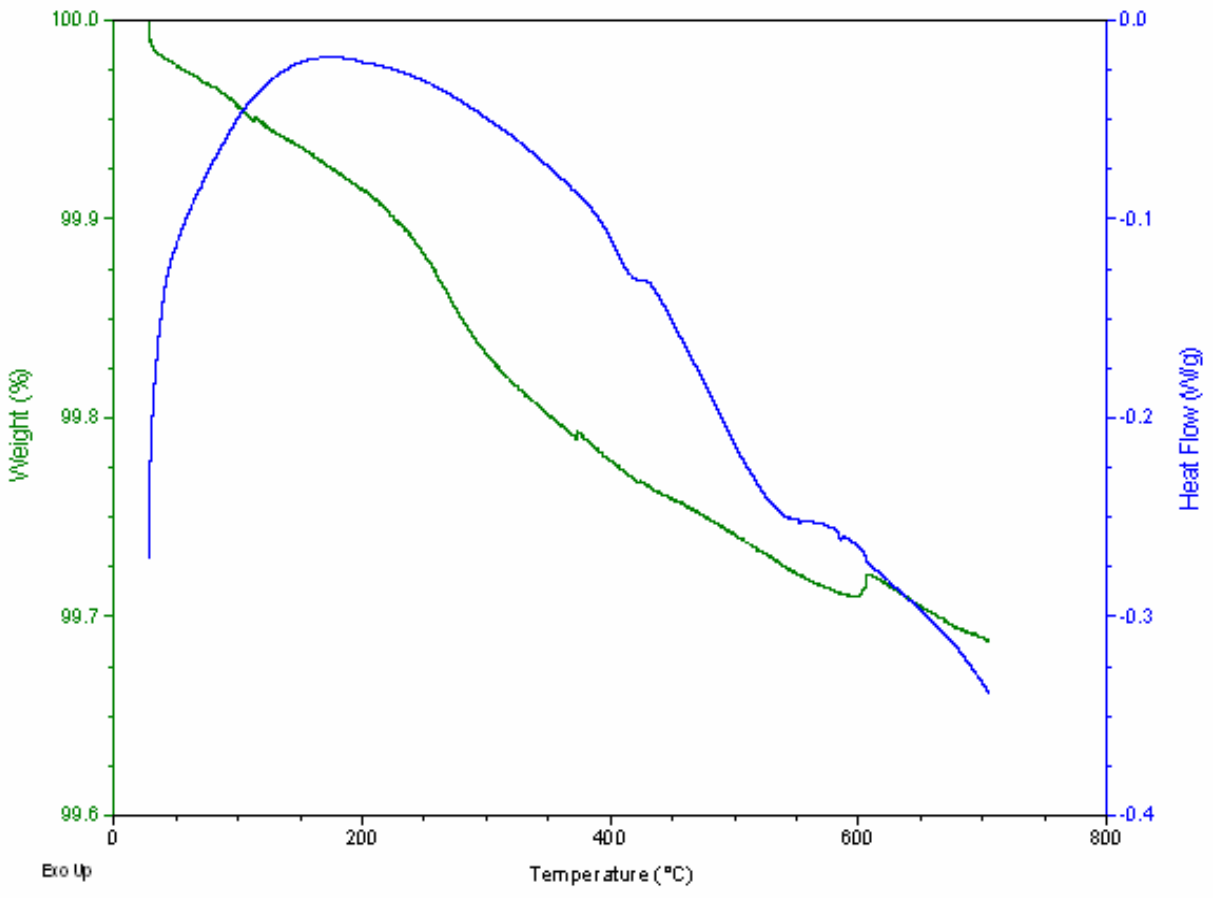

Figure 5.11: *DSC thermograph for sample* $Bi_{3.7}La_{0.3}V_2O_{11}$

DSC-TGA

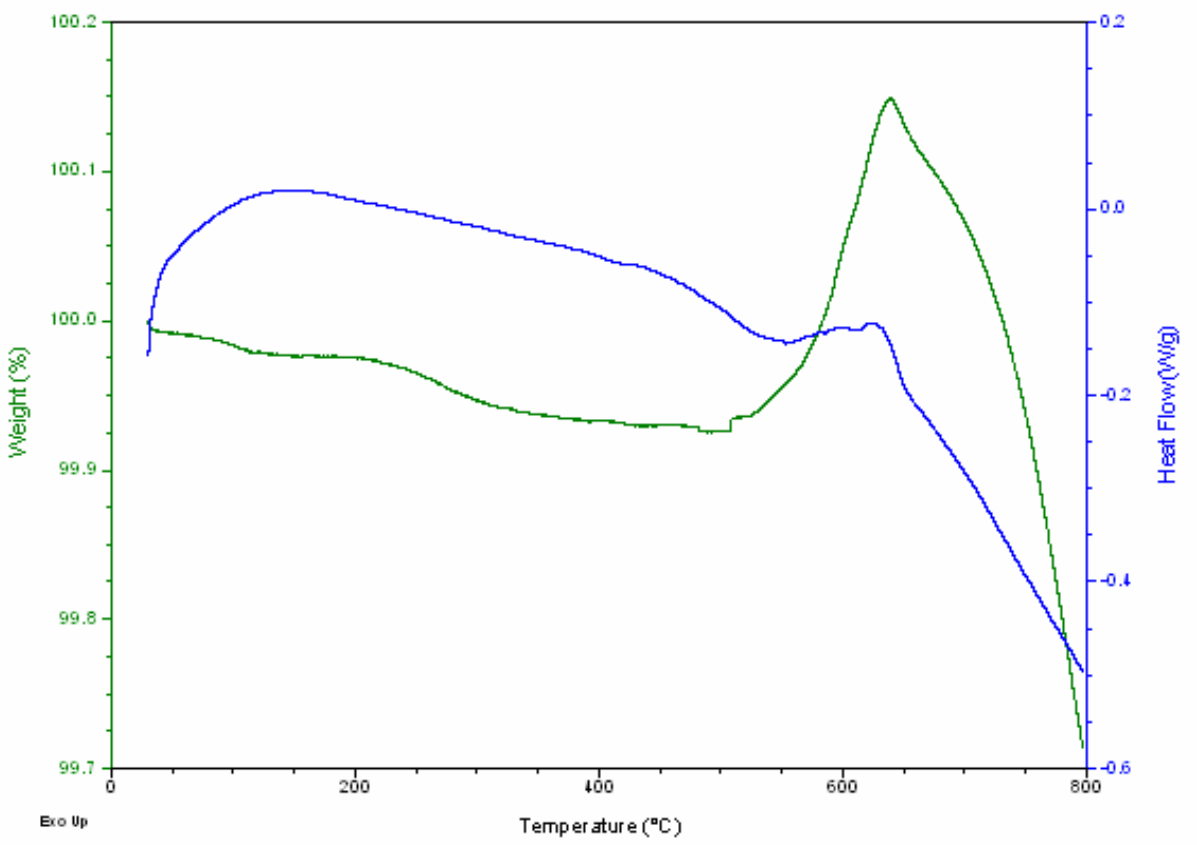

Figure 5.12: *DSC thermograph for sample* $Bi_{3.6}La_{0.4}V_2O_{11}$

DSC-TGA

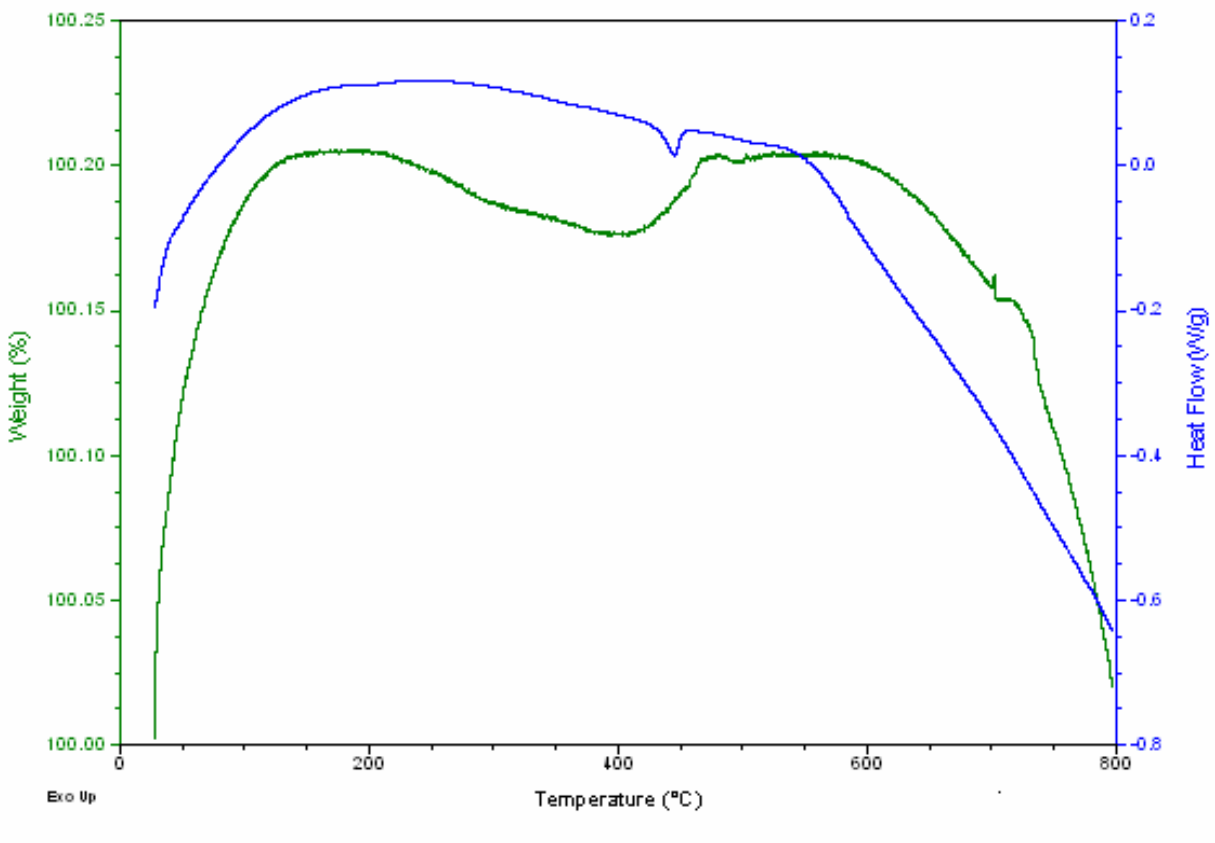

Figure 5.13: *DSC thermograph for sample* $Bi_{3.9}Gd_{0.1}V_2O_{11}$

DSC-TGA

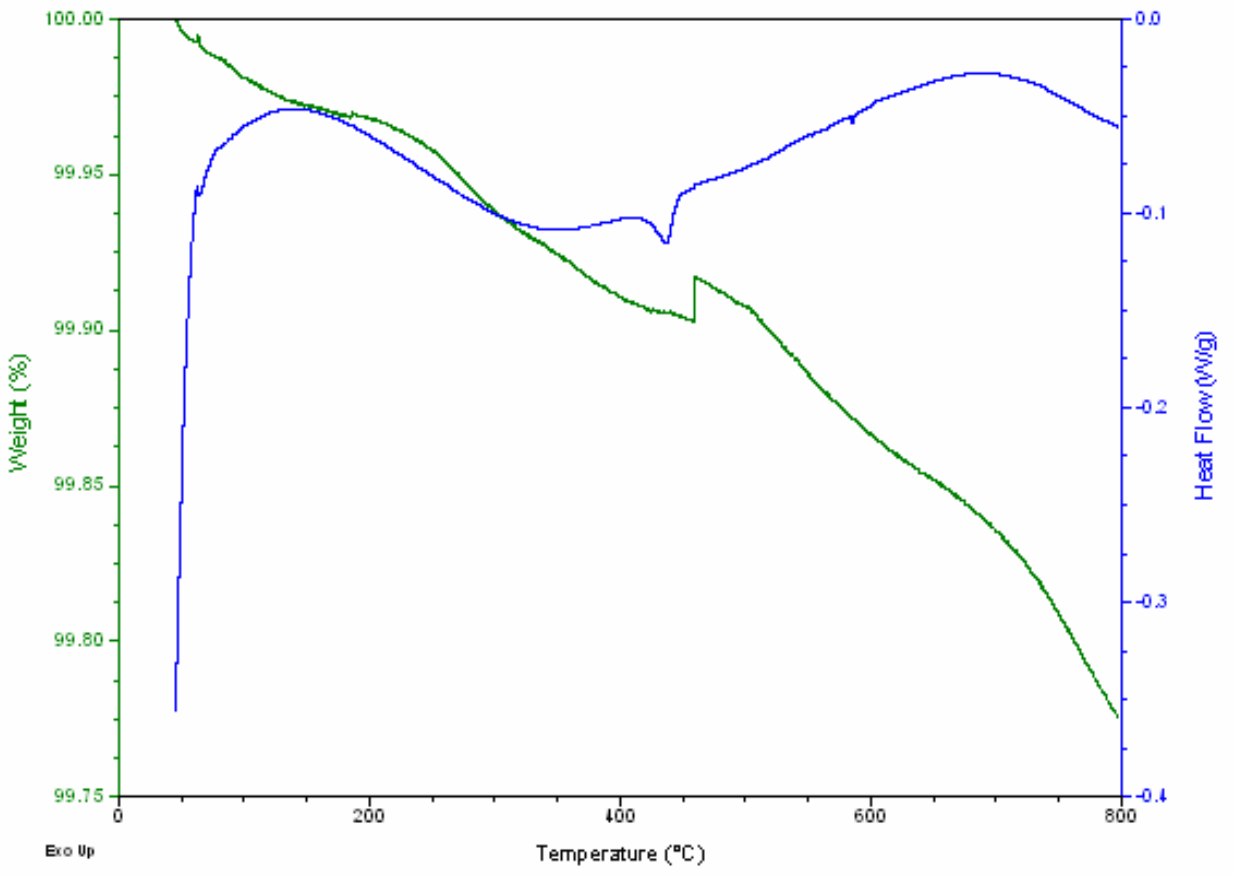

Figure 5.14: *DSC thermograph for sample* $Bi_{3.8}Gd_{0.2}V_2O_{11}$

DSC-TGA

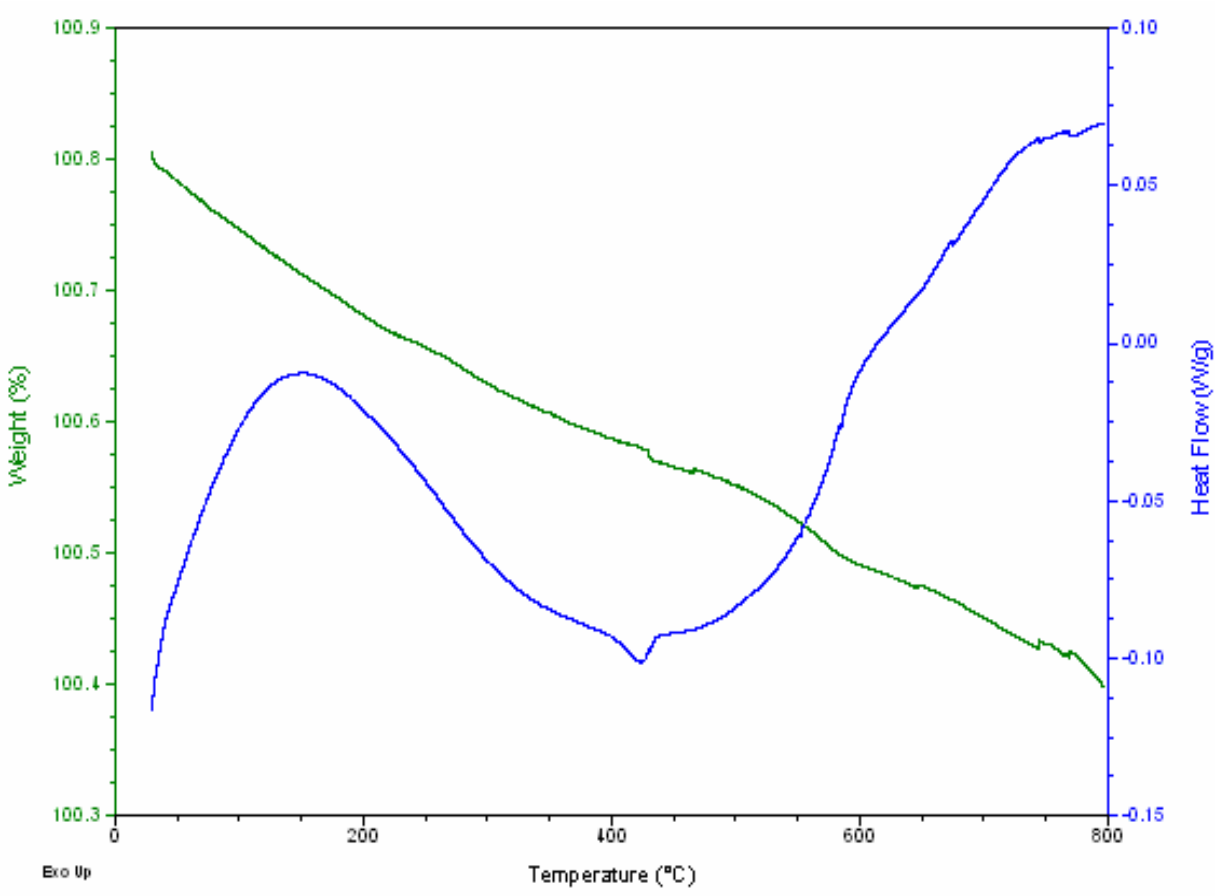

Figure 5.15: *DSC thermograph for sample* $Bi_{3.7}Gd_{0.3}V_2O_{11}$

DSC-TGA

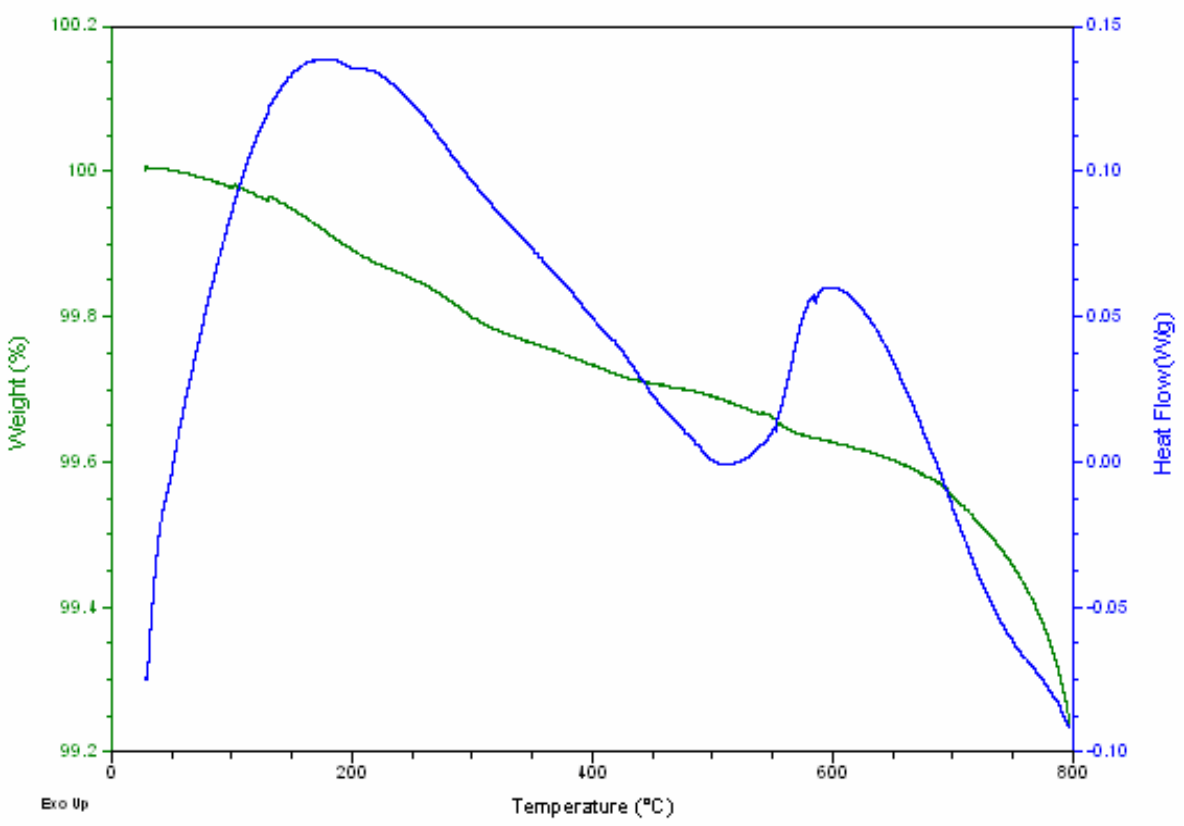

Figure 5.16: *DSC thermograph for sample* $Bi_{3.6}Gd_{0.4}V_2O_{11}$

5.3 Conductivity Measurements

The general features of the impedance spectra and their evolution with temperature are similar for all samples. At low temperature, the impedance spectra consist of one semicircle by which the contributions of the bulk sample and grain boundaries could not be distinguished. However, some spectra exhibit asymmetry at the low frequency range which suggests a grain boundary contribution. As the temperature increases, the resistance decreases and higher frequencies are required to measure complete semicircles due to the total conductivity (bulk and grain boundary contributions). Due to the limitation of applied frequency in the present setup the semicircle corresponding to the bulk conductivity is not found. At 700^{o}C, a spike at very low frequencies associated with the polarization of electrodes is also observed. The low frequency spike suggests that the compound is primarily an ionic conductor [43]. The total sample resistance at each temperature was determined from the intersection point of the spectrum with the real axis and converted into conductivity using $\sigma = L/AR$ (S cm^{-1}) where L is the pellet thickness and A is the pellet crossectional area. Detailed conductivity studies were carried of $Bi_{4-x}M_xV_2O_{11}$ (M=La, Gd; $0 \leq x \leq 0.4$) samples with respect to temperature and frequency.

The data for x=0.1, 0.2, 0.3 and 0.4 were measured with a 20 mm pellet are shown in figure 5.25 to 5.33 for both lanthanum and gadolinium systems as plots of log (σ) versus 1000/T. The results of the impedance spectroscopy measurement on gold sputtered pellets showed that when the concentration varies from (0.025 to 1%) the ionic conductivity doesnot change very much on heating, but is increased on cooling by more than one order of magnitude. Some typical conductivity values at various temperatures are given in Fig. 5.26 and 5.27. In present study x = 0 sample clearly indicated three region in Arrhenius plot of conductivity due to phase transition of $\alpha \rightarrow \beta$ and $\beta \rightarrow \gamma$. The transitions corresponding to $\alpha \rightarrow \beta$ and $\beta \rightarrow \gamma$ phases are evident both in ionic conductivity plots and in the DSC profiles. In $Bi_{4-x}M_xV_2O_{11}$ (M=La, Gd; $0 \leq x \leq 0.4$) sample showed one transition as evident in DSC profile of these samples. In contrast to Gd dopant samples ($Bi_{3.7}La_{0.3}V_2O_{11}$) shoe two transitions at 400^{o}C and 580^{o}C respectively as evident in DSC profile of this particular sample. The discrepancies as indicated in table 3 in the transition temperatures seen by these two different measurements indicate that the structural changes involved in these transitions are sluggish.

All the substituted samples show significantly higher conductivity than the parent compound. The higher conductivities observed (Fig. 5.26 and 5.27) for the substituted samples of $Bi_{4-x}M_xV_2O_{11}$ ($0 \leq x \leq 0.3$) compared with that of parent compound are primarily due to the higher disordering created by the dopant. The x = 0.4 samples also show higher ionic conductivity than the parent compound it might be due to β-phase transition [33].

The ionic conductivity of $Bi_{4-x}La_xV_2O_{11}$ (Fig. 5.26) increases with increasing concentrations of La upto x = 0.1. the sharp decrease of ionic conductivity seen for the samples with x = 0.2, 0.3 is attributed to either defect pair formation or the possibility that the true solid solution formation range of La-substituted phase is $x \leq 0.1$(i.e. the concentration of impurity phases is too small to be detected by XRD).

In comparison of both the series of samples, the change in unit cell volume of La doped samples are less than Gd doped samples. Unit cell of x = 0.1 La doped sample is less than x = 0.2 and x = 0.3 sample having higher conductivity than other doped samples. The difference between ionic conductivity of La-doped and Gd-doped samples may be attributed due to effective ionic radii difference among parent and doped (La, Gd) samples.

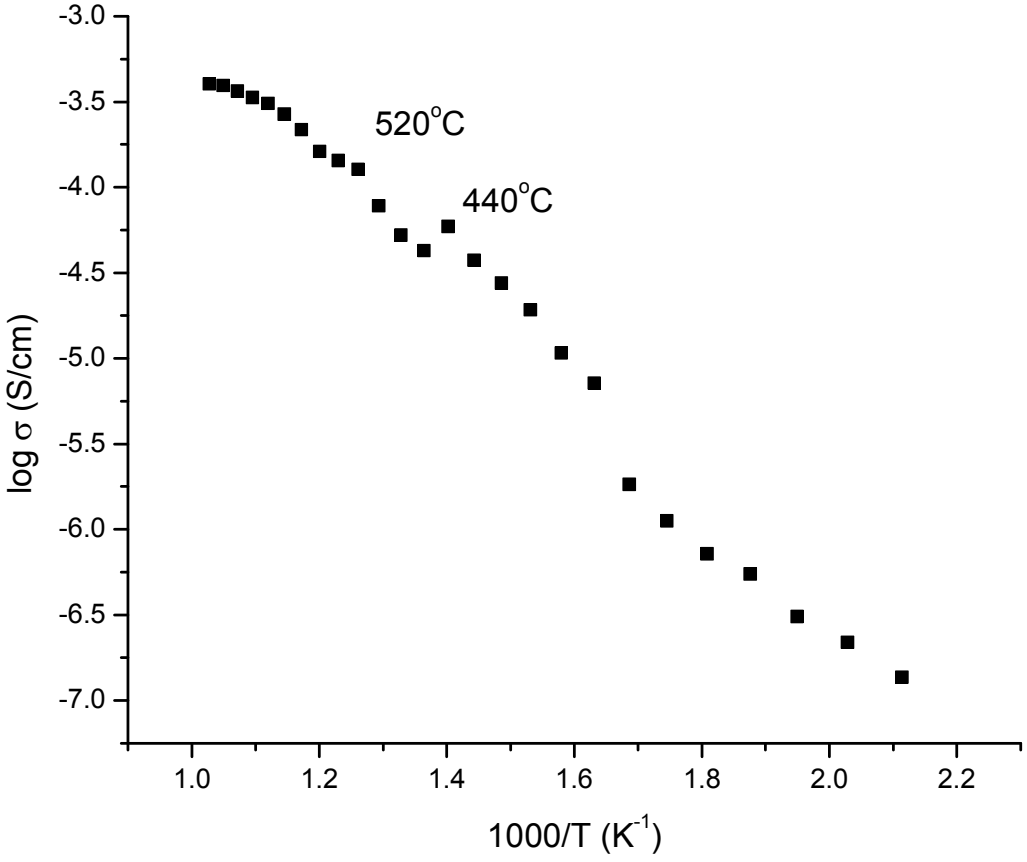

Figure 5.17: *Arrhenius plot of the conductivities of the $Bi_4V_2O_{11}$ taken during cooling*

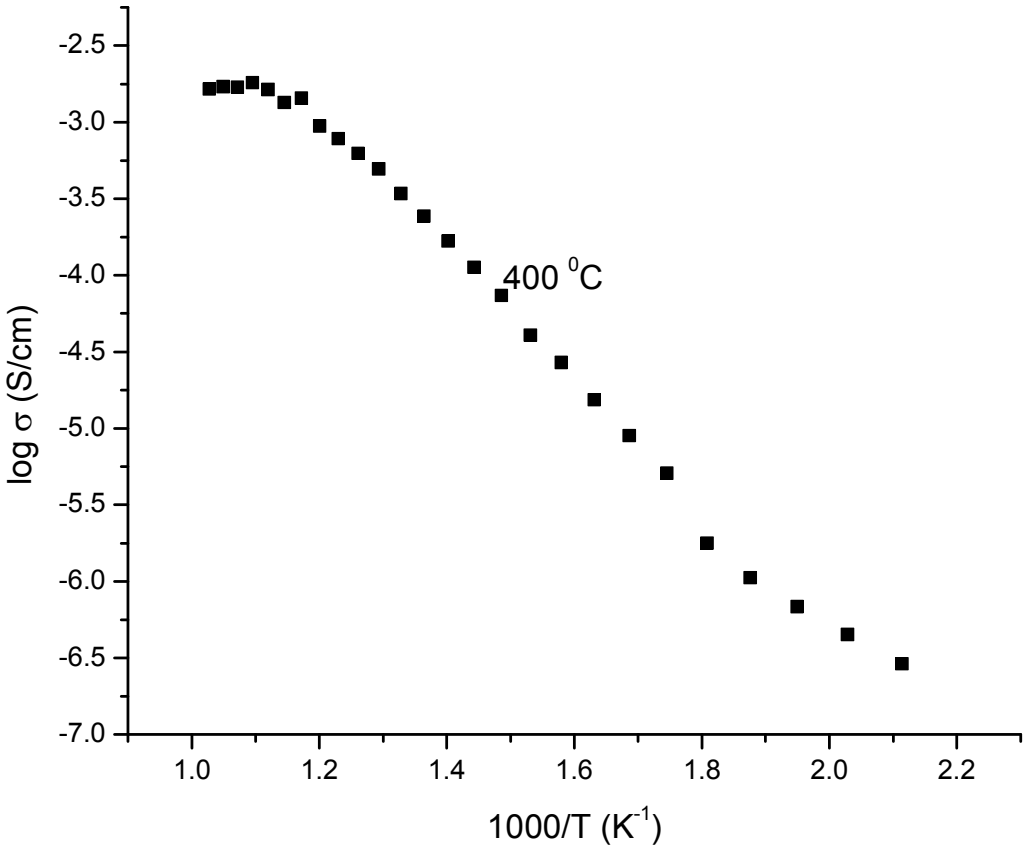

Figure 5.18: *Arrhenius plot of the conductivities of the $Bi_{3.9}La_{0.1}V_2O_{11}$ taken during cooling*

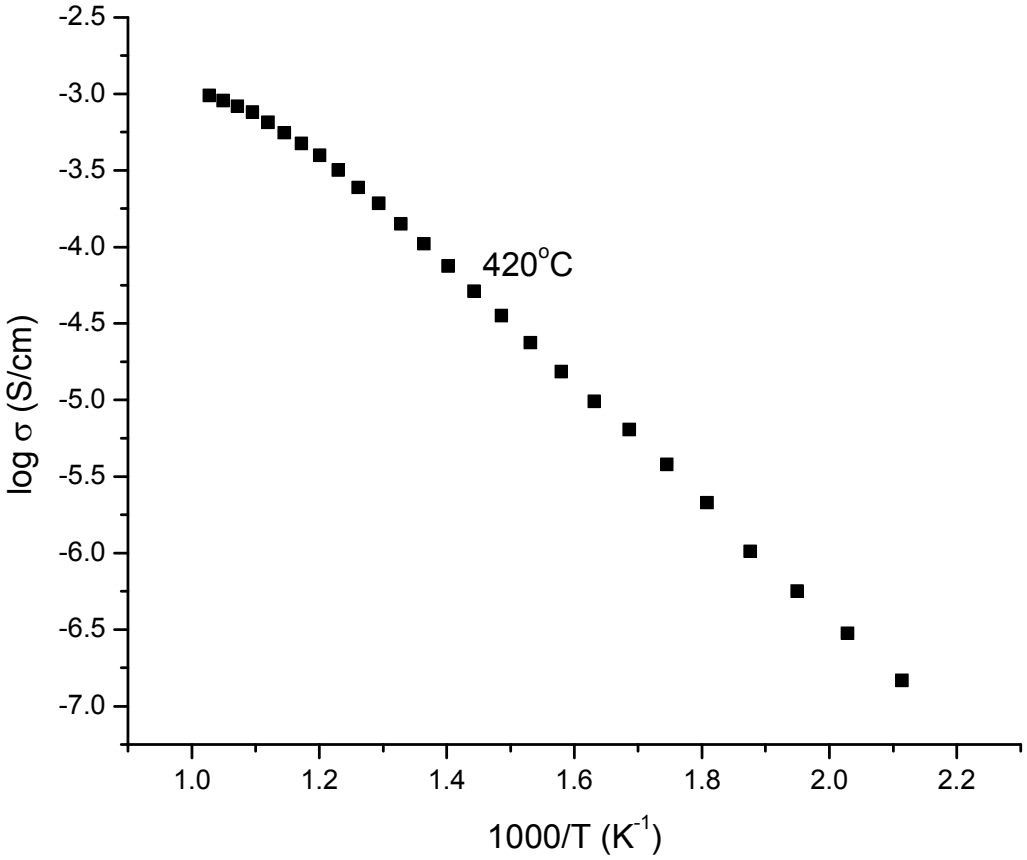

Figure 5.19: *Arrhenius plot of the conductivities of the $Bi_{3.8}La_{0.2}V_2O_{11}$ taken during cooling*

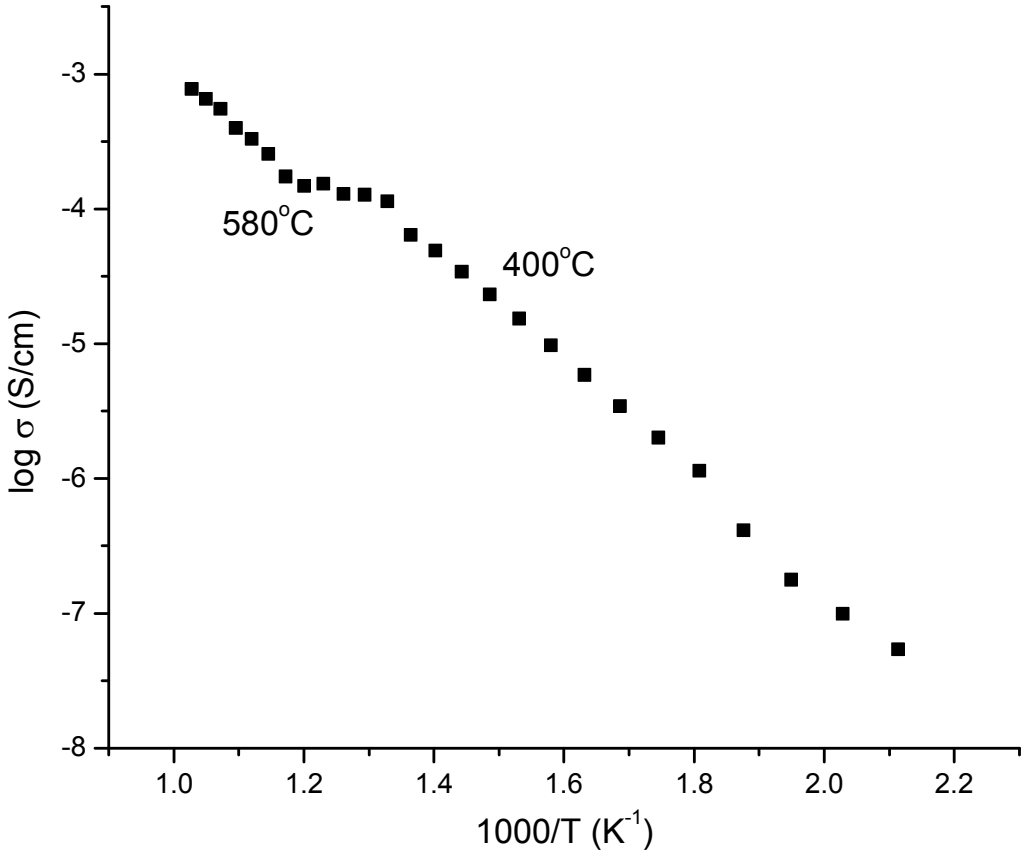

Figure 5.20: *Arrhenius plot of the conductivities of the $Bi_{3.7}La_{0.3}V_2O_{11}$ taken during cooling*

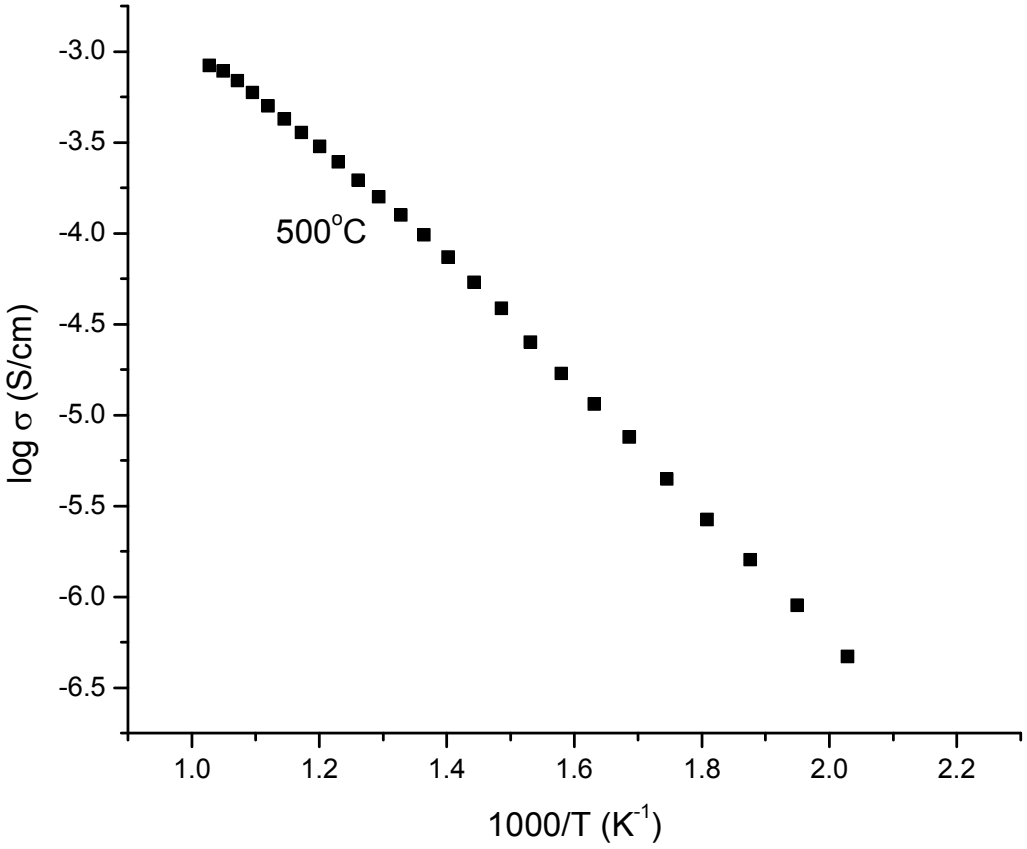

Figure 5.21: *Arrhenius plot of the conductivities of the $Bi_{3.6}La_{0.4}V_2O_{11}$ taken during cooling*

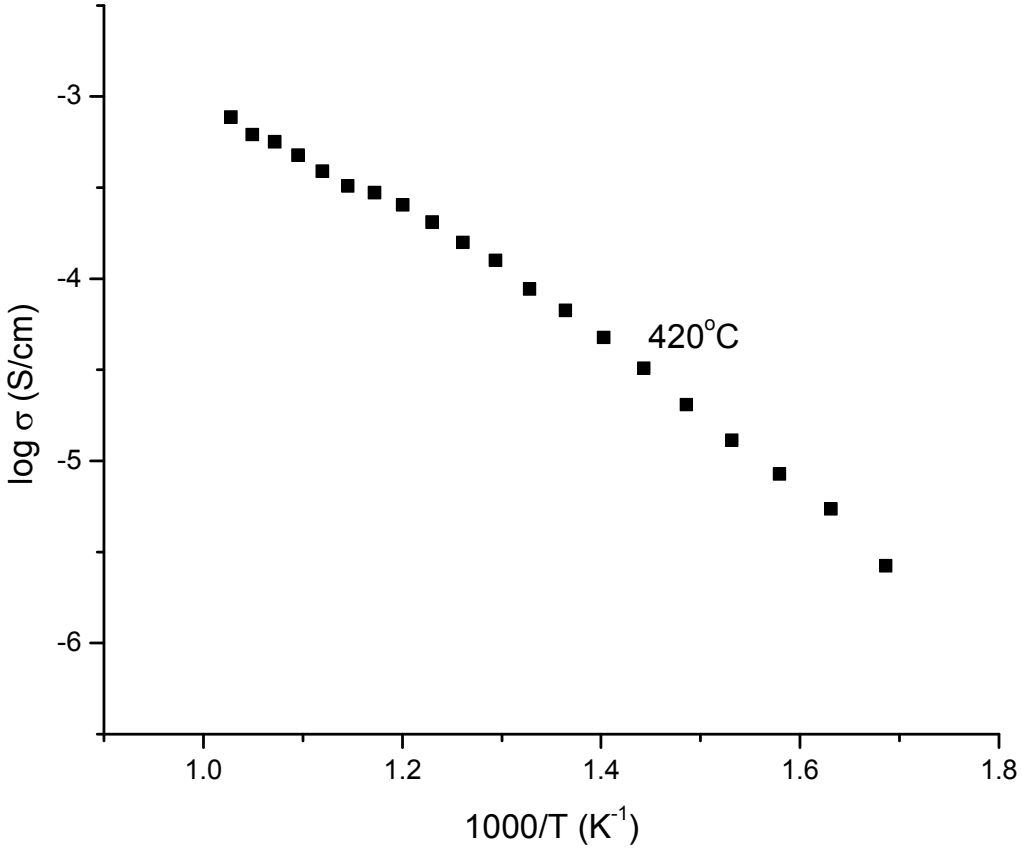

Figure 5.22: *Arrhenius plot of the conductivities of the $Bi_{3.9}Gd_{0.1}V_2O_{11}$ taken during cooling*

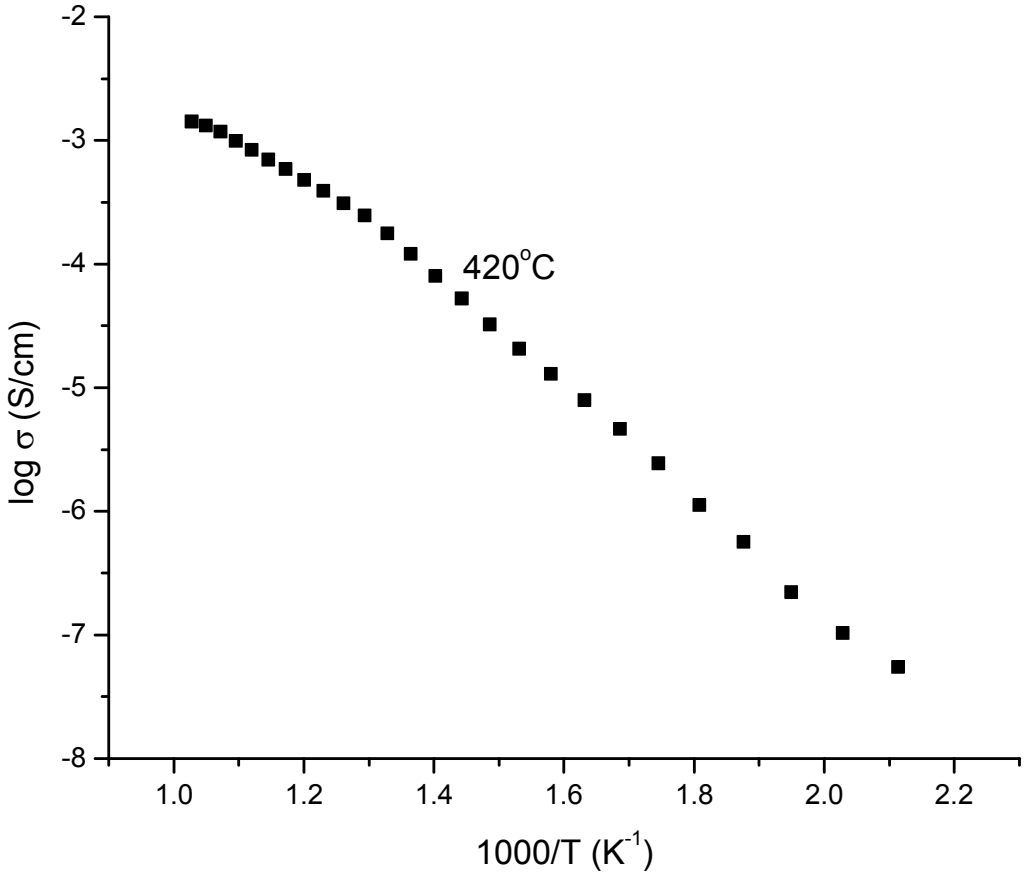

Figure 5.23: *Arrhenius plot of the conductivities of the $Bi_{3.8}Gd_{0.2}V_2O_{11}$ taken during cooling*

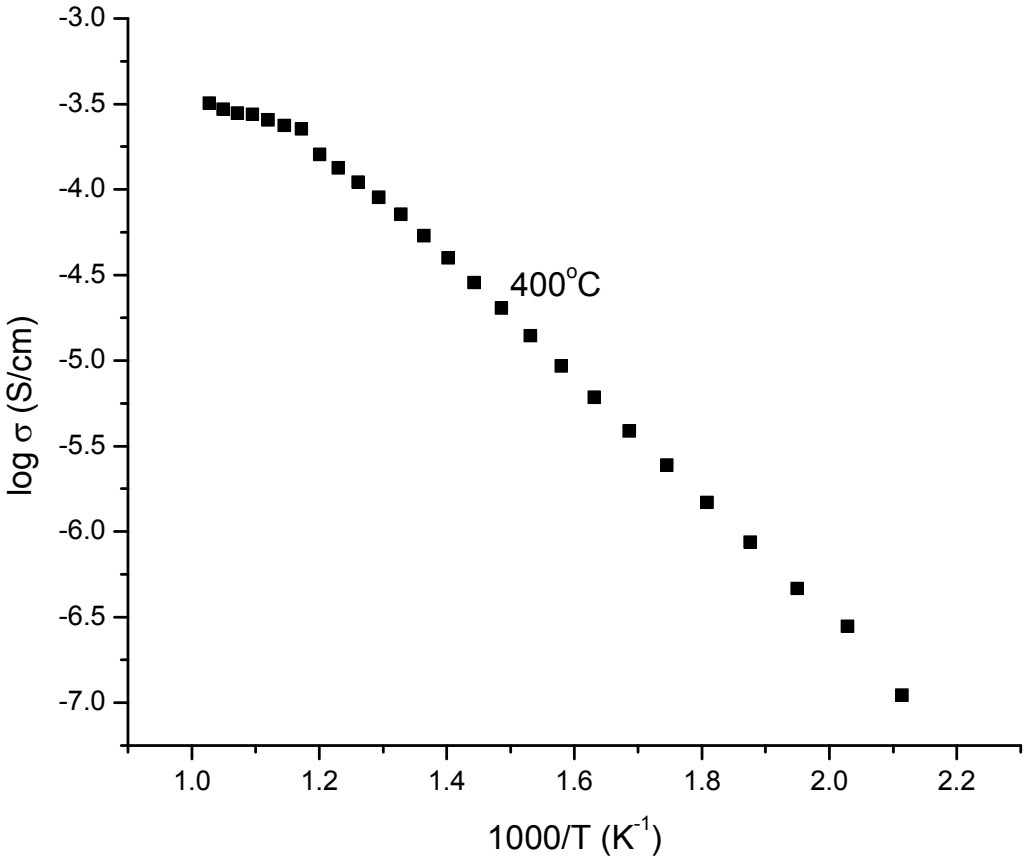

Figure 5.24: *Arrhenius plot of the conductivities of the $Bi_{3.7}Gd_{0.3}V_2O_{11}$ taken during cooling*

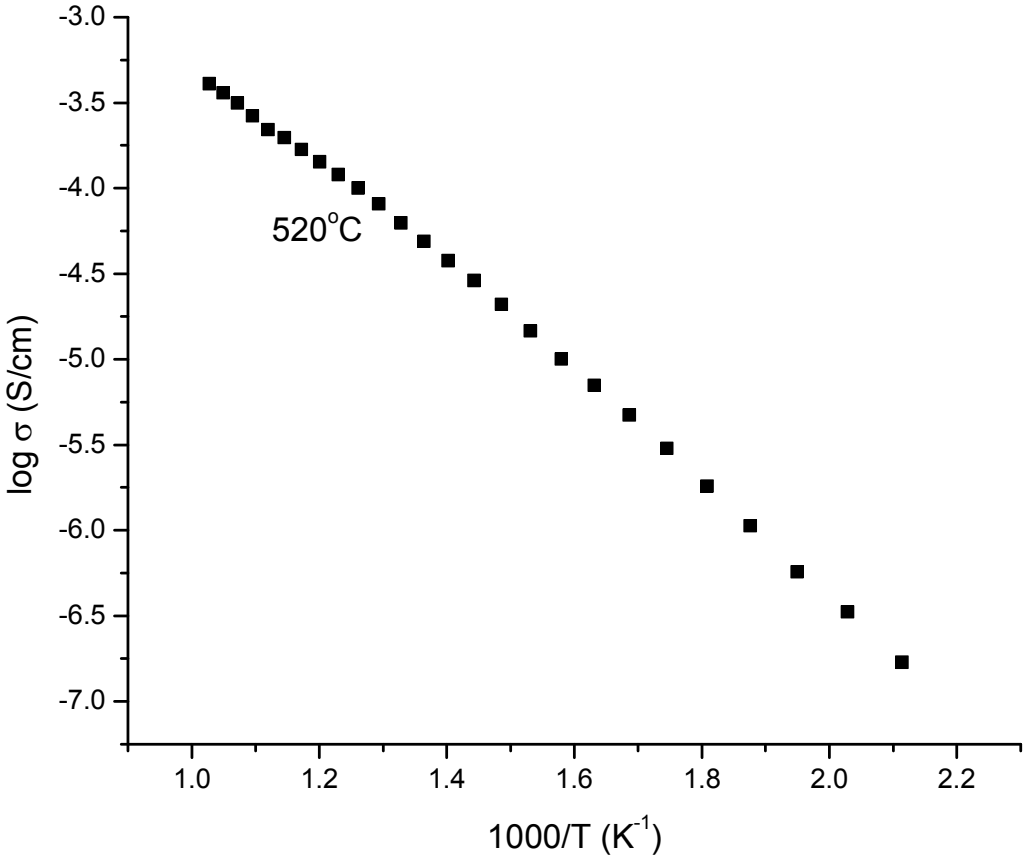

Figure 5.25: *Arrhenius plot of the conductivities of the $Bi_{3.6}Gd_{0.4}V_2O_{11}$ taken during cooling*

Table 3: Phase transition temperatures for $Bi_{4-x}La_xV_2O_{11}$ (x=0, 0.1, 0.2, 0.3 and 0.4) obtained from ac conductivity and DSC measurement

Composition x	**Phase transition temperature from ac conductivity(^oC)**	**Phase transition temperature from DSC(^oC)**
x =0	440 520	440 520
x =0.1	400	420
x = 0.2	420	410
x = 0.3	400 580	400 580
x = 0.4	500	520

Table 4: Phase transition temperatures for $Bi_{4-x}Gd_xV_2O_{11}$ (x=0, 0.1, 0.2, 0.3 and 0.4) obtained from ac conductivity and DSC measurement

Composition x	**Phase transition temperature from AC conductivity(^oC)**	**Phasetransition temperature from DSC(^oC)**
x =0	440 520	440 520
x =0.1	420	420
x = 0.2	420	410
x = 0.3	400	400
x = 0.4	520	500

The dependence of conductivity data on x is rather complex and is shown in figure 5.26 and 5.27 for both La and Gd systems respectively

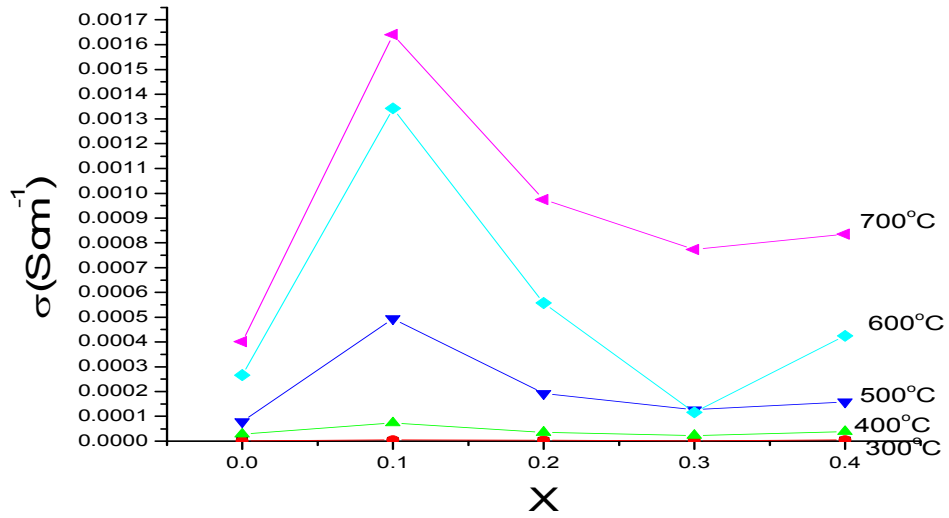

Figure 5.26: *Variation of conductivity at different temperatures with respect to composition x for $Bi_{4-x}La_xV_2O_{11}$ ($0 \leq x \leq 0.4$)*

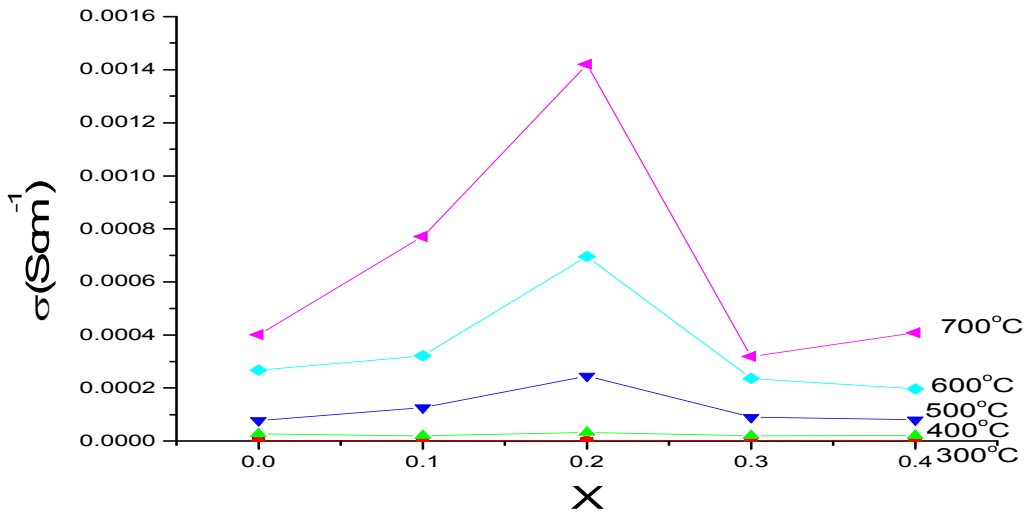

Figure 5.27: *Variation of conductivity at different temperatures with respect to composition x for $Bi_{4-x}Gd_xV_2O_{11}$ ($0 \leq x \leq 0.4$)*

CHAPTER 6

CONCLUSION AND SUGGESTION FOR FUTURE WORK

6.1 CONCLUSION

In the present work, Bi_{4-x} $La_xV_2O_{11}$ and Bi_{4-x} $Gd_xV_2O_{11}$ ($0 \leq x \leq 0.4$) electrolytes were synthesized by solid-state reaction process. According to the X-Ray diffraction pattern the first three compositions in both systems exhibited α-phase except some peak broadening or peak shifting. XRD peak broadening and shifting in the substituted samples has been attributed mainly to the disordering and strain introduced through La^{3+} and Gd^{3+} doping for Bi^{3+} in parent sample. The high temperature β-phase of $Bi_4V_2O_{11}$ is stabilized for Bi_{4-x} $M_xV_2O_{11}$ with M = Gd, La and $x \geq 0.4$. The phase transition corresponding to α→β and β→γ phases are evident in the ionic conductivity plots and in the DSC profiles of pure $Bi_4V_2O_{11}$ sample. All other dopant samples exhibit only one transition temperature in both the measurement except $Bi_{3.7}$ $La_{0.3}V_2O_{11}$ sample. The discrepancies in the transition temperatures seen by these two measurements indicate that the structural changes involved in these transitions are sluggish. The increased ionic conductivity of the substituted phases compared to the parent compound may be attributed to the increased disorder and strain created by the substitution (Gd, La) for Bi and ionic radii of these cations.

6.2 Suggestion for Future work

For γ-phase stabilization at room temperature in $Bi_4V_2O_{11}$ compound which is highly disorder and highly ionic conducting will be stabilized to substitute higher concentration of Gd^{3+} and La^{3+}. Apart from this lower and higher valence cation for Bi^{3+} in $Bi_4V_2O_{11}$ system, can be substituted to stabilize γ-phase at room temperature. Ionic conductivity of these samples with respect to time can also be done to check the stability of the phases in various temperature ranges. After confirmation of γ-phase stabilization, its compatibility can be investigated with the other components of SOFC such as glass sealants.

REFERENCES

REFERENCES

[1] Anthony R.West, Solid State Chemistry and its Applications, John Wiley & Sons Ltd.(1984).

[2] J.B. Goodenough, Annu.Rev.Mater.Res.33 (2003), 91-128.

[3] W.R. Grove, Phillos.Mag.41 (1839), 127-30.

[4] W. Nernest, Z. Elekrochem. 6 (1899), 41-43.

[5] E. Baur, H. Presis, Z. Elekrochem.43 (1937), 727-32.

[6] L. Carrette, K.A. Friedrich, U. Stimming, Chemphyschem, 1 (2000), 162-193.

[7] Nguyen Q. Minh, J.Am.Ceram.Soc. 76 (3) (1993), 563-88.

[8] "Proceedings of the Grove Anniversary Fuel Cell Symposium", Royal Institution, London, 18-21 September 1989 (Elsevier, Amsterdam, 1990).

[9] S. Srinivasan, F. J. Salzano and A.R. Landgrebe (eds), "Industrial Water Electrolysis", (The Electrochemical Society, Princeton, NJ, 1978).

[10] K. Kendal, Am.Ceram.Soc.Bull. 70 (1991),1159.

[11] T. Sato, M. Ishitsuka, T. Fukushima, T. Endo and M. Schimada, Mater.Sci.Forum 34-36 (1988), 189.

[12] H. Yahiro, Y. Baba, E. Eguchi and H. Arai, ibid. 135 (1988),2077.

[13] R.L. Cook, R.C. MacDuff and A.F. Sammells, J.Electrochem.Soc. 137 (1990),3309.

[14] R.L. Cook, J.J. Osborne, J.H. White, R.C. MacDuff and A.F. Sammells,

J.Electrochem.Soc. 139 (1992), L19.

[15] H. Iwahara, T. Esaka, H. Uchida and N. Maeda, Solid State Ionics 3-4 (1981), 359.

[16] A.M. Azad, S. Larose, S.A. Akbar, J. Materials Science 29 (1994), 4135-4151.

[17] I.Abrahams, A.J. Bush, F. Krok, G.E. Hawkes, K.D. Sales, P. Thornton and W. Bogusz, J. Mater.Chem.,8(5) (1998), 1213-1217.

[18] X.J. Chen, K.A. Khor, S.H. Chan and L.G. Yu, J. Mater. Science and EngineeringA, 335, 1-2, (2002), 246-252.

[19] C. Brahim, A. Ringuede, E. Gourba, M. Cassir, A. Billard and P. Briois, J. Power Sources, (2005),1010-1016.

[20] Q. Zhu and B. Fan, J. Solid State Ionics, 176, 9-10, (2005), 889-894.

[21] I.R. Gibson, G.P. Dransfield and J.T.S. Irvine, J. European Ceramic Society, 18, 6, (1998), 661-667.

[22] M. Hattori, Y. Takeda, Y. Sakai, A. Nakanishi, S. Ohara, K. Mukai, J.H. Lee and T. Fukui, J. Power Sources, 129, 2, (2004), 188-192.

[23] M.D. Anderson, J.W. Stevenson and S.P. Simner, J. Power Sources, 129, 2, (2004), 1888-192.

[24] M.D. Ridder, A.G.J. Vervoort, R.G.V. Welzenis and H.H. Brongersma, J. Solid State Ionics, 156, 3-4, (2003), 225-262.

[25] N.M. Sammes and Z. Cai, J. Solid State Ionics, 100, 1-2, (1997), 39-44.

[26] Naixiong Jiang, Eric D WAchsman, Su-Ho Jung, J. Solid State Ionics, 150 (2002), 347-353.

[27] J.C.Boivin, J. Inorganic Materials, 3, (2001), 1261-1266.

[28] J.C. Boivin, C. Pirovano, G. Nowogrocki, G. Mairesse, Ph. Labrune and G. Lagrange, J. Solid State Ionics, 113,115 (1998), 639-651.

[29] J.R. Dygas, P. Kurek and M.W. Breiter, J. Electrochimica Acta, 40, 10, (1995), 1545-1550.

[30] P.Q. Pho and V.T. Son, Abstract. Vietnamese Seminar on Physics and Engg. (2001), 1550-1555.

[31] S.P.Simner, D.S. Sandoval, J.D. Mackenzie and B. Dunn, J.Am.Ceram.Soc.80, 10, (1997), 2563-2568.

[32] R.N.Vannier, G. Mairesse, G. Nowogrocki, F. Abraham and J.C. Boivin, J. Solid State Ionics, 53, 56, 2 (1992), 713-722.

[33] E.Pernot, M. Anne, M. Bacmann, P, Strobel, J. Solid State Ionics, 70/71 (1994) 259-263.

[34] O. Joubert, M. Ganne, R.N. Vannier, G. Mairesse, J. Solid State Ionics, 83 (1996), 199-207.

[35] A.A. Yaremchenko, V.V. Kharton, E.N. Naumovich, A.A. Tonoyan, Materials Research Bulletin 35 (2000) 515–520.

[36] I. Abrahams and F. Krok, J. Mater. Chem., 12 (2002), 3351-3362.

[37] J. Yan and M. Greenblatt, J. Solid State Ionics, 81 (1995), 225-233.

[38] R.N. Vannier, G. Mairesse, F. Abraham, G. Nowogrocki, J. Fouletier and M. Bacmann, J. Solid State Ionics, 78, (1995), 183-189.

[39] C.K. Lee, D.C. Sinclair and A.R. West, J.Solid State Ionics, 62 (1993), 193-198.

[40] C.K. Lee, C.S. Ong, J. Solid State Ionics, 117 (1999), 301–310.

[41] K.Z Fung and A.V. Virkar, ibid. 74 (1991),1970.

[42] S.N. Achary, M.D. Mathews, S.J. Patwe and A.K. Tyagi, J. Materials Science Letters, 18 (1999), 335-357.

[43] L. Qiu, Y.L. Yang and A.J. Jacobson, J. Mater. Chem., 7(2), (1997), 249-253.

[44] N.M. Sammes, G.A. Tompsett, H.N. Fea and F. Aldingera, J. European Ceramic Society, 19 (1999), 1801-1826.